Supporting Information

Rational design of a ratiometric two-photon fluorescent probe for real-time visualization of apoptosis

Yinliang Huang,[1a] Qin Zhou,[1b] Yan Feng,*[a] Wan Zhang,[a] Guoshun Fang,[a] Min Fang,[a] Man Chen,[a] Changzhi Xu,*[b] Xiangming Meng*[a, c]

[a.] *School of Chemistry and Chemical Engineering & Center for Atomic Engineering of Advanced Materials & AnHui Province Key Laboratory of Chemistry for Inorganic/Organic Hybrid Functionalized Materials, Anhui University, Hefei 230601, P.R. China. E-mail: fy70@163.com (Yan Feng), mengxm@ahu.edu.cn (Xiangming Meng).*

[b.] *Institute of Health Sciences, Anhui University, Hefei 230601, P.R. China. E-mail: changzhixu007@163.com (Changzhi Xu);*

[c.] *Institute of Physical Science and Information Technology, Anhui University, Hefei 230601, P.R. China.*

[1] *Both authors contributed equally to this work.*

List of contents

1. Theoretical calculation

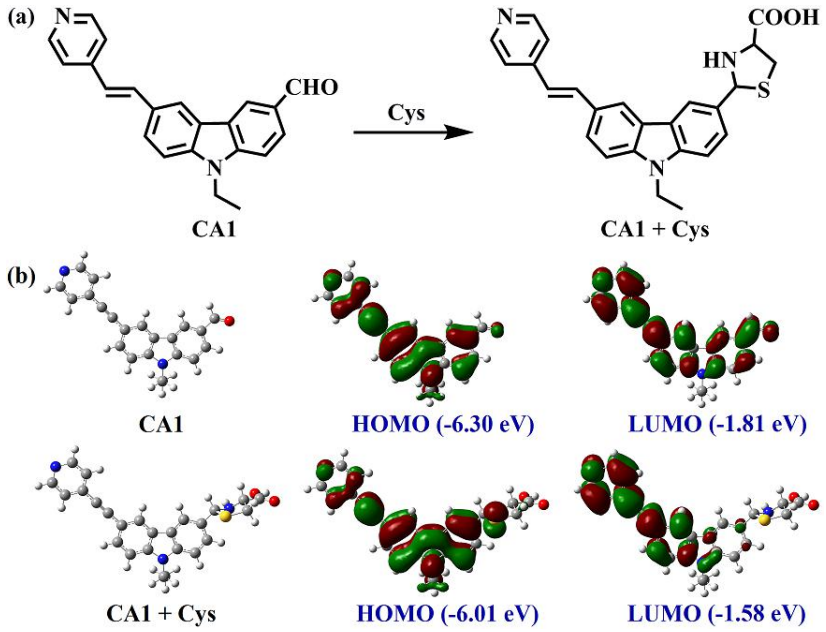

Fig. S1 (a) Reaction of **CA1** with Cys. (b) Calculated **HOMO** and **LUMO** of **CA1** and **CA1 + Cys** .

To better understand the behavior of three probes for sensing Cys, DFT calculations using the M06-D3 method and the def2-SVP basis set with the Gaussian 09 program package have been carried out.[1,2]

As shown in Scheme 1A and Fig. S1, electrons were mainly centralized at the carbazole framework as the donor (D) at the ground state and transferred to the pyridine moiety (A2, as the major part) and aldehyde group (A1, as the minor part) as the acceptors after excitation, indicating a "A2-π-D-π-A1"-typed two-dimensional ICT process for **CA1**. After **CA1** reacting with Cys to obtain product **CA1**+Cys, the electrons were still localized over the carbazole at the ground state, which transferred to the pyridine moiety (A2) only at the excitation state. The result indicated the main ICT system between carbazole and pyridine was unchanged before and after CA1 reacting with Cys. At the sametime, the energy gap between the HOMO and LUMO of CA1 was calculated to be 4.49 eV and that of its product was 4.43 eV. There are

very small differences between two energy gap values, indicating a weak ICT efficiency changes in this reaction. Therefore, we envisioned that the fail of the ratiometric response of **CA1** to Cys was endowed to the remaining of strong ICT efficiency between carbazole and pyridine moieties.

On the other hand, for our probe **Mito-DCHO**, the DFT calculations showed the different results. As shown in Scheme 1A and Fig. S2, electrons were mainly centralized at the carbazole framework as the donor (D) at the ground state and transferred to the two aldehyde groups (A1) as the acceptors after excitation, indicating a "A1-π-D-π-A1"-typed two-dimensional ICT process for **Mito-DCHO**. After the reaction of probe with Cys to obtain product **Mito-DCHO-Cys**, electrons distribution of **Mito-DCHO-Cys** changed to a large extent. The electrons were mainly localized over the carbazole and phenylacetylene group both at the ground and excitation state, which indicated its two-dimensional ICT system was off. Moreover, the energy gap between the HOMO and LUMO of **Mito-DCHO** was calculated to be 3.86 eV and that of **Mito-DCHO-Cys** was 4.24 eV. There are much bigger differences between two energy gap values, indicating a strong ICT efficiency changes happened. More importantly, the strong ICT efficiency changes endowed **Mito-DCHO** with ratiometric fluorescent response to Cys along with a large emission shift (119 nm). **Mito-SCHO** had the similar DFT calculation results. Its fluorescent signal for Cys was consistent with that of **Mito-DCHO** to Cys. However, **Mito-SCHO** with a one-dimensional ICT system cannot discriminate Cys over Hcy for their similar reaction kinetics.

As a result, the DFT calculation supported our rational design that a dialdehyde-functionalized carbazole derivative can serve as a Cys-specific ratiometric fluorescent probe employing a symmetric two-dimensional ICT system.

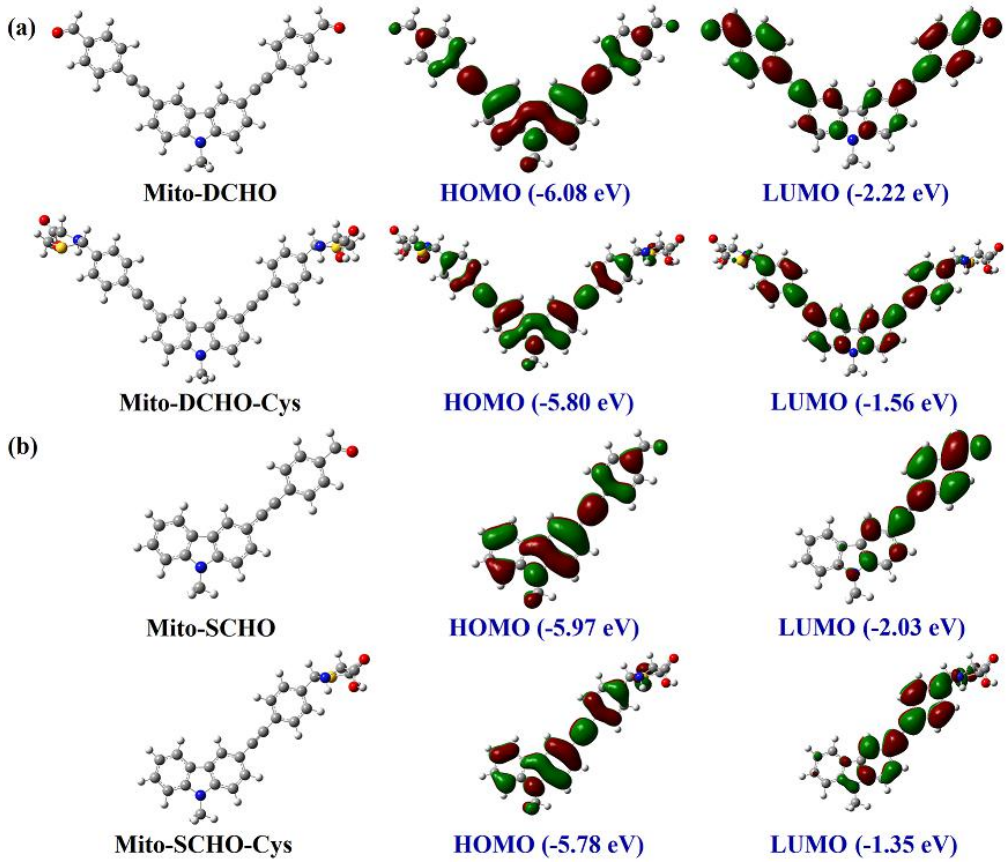

Fig. S2 (a) Calculated **HOMO** and **LUMO** of **Mito-DCHO** and **Mito-DCHO-Cys**. (b) Calculated **HOMO** and **LUMO** of **Mito-SCHO** and **Mito-SCHO-Cys**.

2. Synthesis of **Mito-SCHO** and **Mito-DCHO**

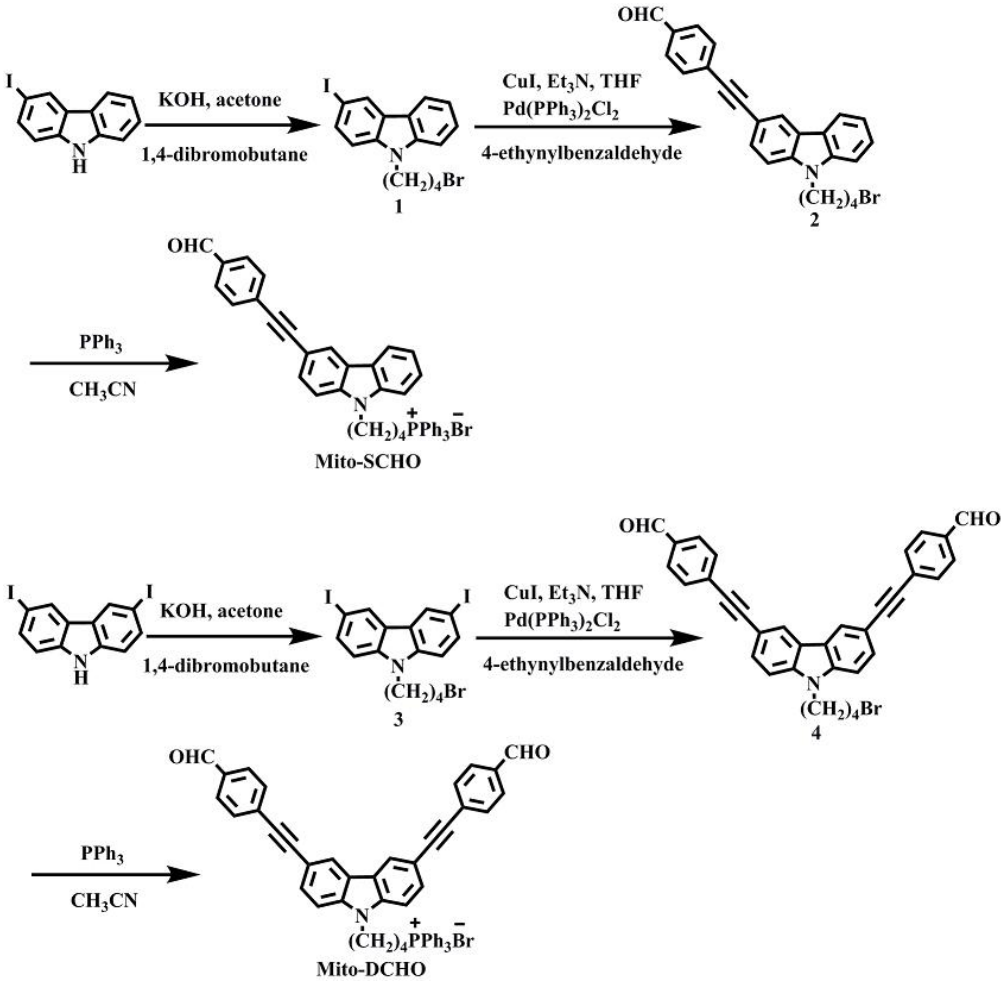

Scheme S1 Synthesis route of **Mito-SCHO** and **Mito-DCHO**.

2.1 Synthesis of compound **1**

A mixture of KOH (2.88 g, 51.4 mmol), KI (0.57 g, 3.4 mmol) and 1,4-dibromobutane (11.1 g, 51.4 mmol) was heated to 60 ^{o}C. After reacting 1h, 3-iodocarbazole (10 g, 34.3 mmol) was added slowly, and the result mixture was refluxed until TLC showed no raw material existed (about 12 h). After cooling to room temperature, 200 mL H_2O was added, and the mixture was extracted with dichloromethane (100 mL×2). The organic phase was evaporated to give crude product. The crude material was purified by column chromatography (petroleum ether:dichloromethane = 10 : 1 as the eluent) to give 6.4 g (43.6%) of **1**.

^{1}H NMR (400 MHz, $CDCl_3$, ppm): δ 8.39 (s, 1H), 8.03 (d, *J* = 7.8 Hz, 1H), 7.70 (d, *J* = 8.7 Hz, 1H), 7.49 (t, *J* = 7.6 Hz, 1H), 7.39 (m, *J* = 8.1 Hz, 1H), 7.24 (t, *J* = 10.9 Hz, 1H), 7.18 (d, *J* = 8.5 Hz, 1H), 4.32 (t, *J* = 6.8 Hz, 2H), 3.37 (t, *J* = 6.4 Hz, 2H), 2.04 (m, *J* = 14.5, 7.4 Hz, 2H), 1.89 (m, *J* = 13.2, 6.6 Hz, 2H). ^{13}C NMR (100 MHz, $CDCl_3$, ppm): δ 140.27, 139.44, 133.93, 129.30, 126.48, 125.45, 121.67, 120.62, 119.53, 110.60, 108.74, 81.41, 42.27, 32.97, 30.14, 27.55.

2.2 Synthesis of compound **2**

A mixture of compound **1** (1 g, 2.3 mmol), 4-ethynylbenzaldehyde (0.46 g, 3.5 mmol), $Pd(PPh_3)_2Cl_2$ (6.6 mg, 0.009 mmol), CuI (3.6 mg, 0.018 mmol) and Et_3N (5 ml) was stirred at 30 ^{o}C for 12 h under the anhydrous and anaerobic conditions. the mixture was cooled to room temperature. Precipitates were filtered off and concentrated to give the crude product. The crude material was purified by column chromatography (petroleum ether:dichloromethane = 4 : 1 as the eluent) to give 600 mg (59.7%) of **2**.

^{1}H NMR (400 MHz, $CDCl_3$, ppm): δ 9.93 (s, 1H), 8.24 (s, 1H), 8.02 (d, *J* = 7.8 Hz, 1H), 7.78 (d, *J* = 7.5 Hz, 2H), 7.59 (d, *J* = 16.5, 8.0 Hz, 3H), 7.42 (t, *J* = 7.7 Hz, 1H), 7.31 (m, *J* = 14.1, 8.4 Hz, 2H), 7.22-7.16 (t, 1H), 4.25 (m, *J* = 13.1, 6.5 Hz, 2H), 3.30 (t, *J* = 6.5 Hz, 1H), 3.07 (t, *J* = 6.7 Hz, 1H), 2.02-1.90 (m, 2H), 1.87-1.75 (m, 2H). ^{13}C NMR (100 MHz, $CDCl_3$, ppm): δ 191.48, 140.71, 140.33, 135.01, 131.86, 130.37, 129.65, 129.55, 126.47, 124.49, 123.07, 122.48, 120.66, 119.80, 112.64, 108.93, 108.77, 95.38, 87.24, 42.16, 32.97, 27.62, 5.72.

2.3 Synthesis of **Mito-SCHO**

A mixture of **2** (1 g, 2.3 mmol) and acetonitrile (10 ml) was heated to 80 ^{o}C under

the condition of nitrogen. After 1 h, PPh_3 (3.7 g, 13.9 mmol) was added, the result mixture was refluxed until TLC showed no raw material existed (about 36 h). After being cooled to room temperature, the mixture was filtered and the filtrate was evaporated to give the crude product. The crude product was purified through column chromatography (dichloromethane:acetonitrile = 3 : 1 as the eluent) to give 0.96 g (60%) of **Mito-SCHO**. ESI-MS m/z: [**Mito-SCHO** - Br]$^+$ $C_{43}H_{35}NOP^+$ calcd, 612.2456; found, 612.2427.

^{1}H NMR (400 MHz, DMSO-d_6, ppm): δ 10.05 (s, 1H), 8.46 (s, 1H), 8.22 (d, J = 7.9 Hz, 1H), 7.98 (d, J = 7.3 Hz, 2H), 7.87 (t, J = 6.5 Hz, 3H), 7.79 (d, J = 7.5 Hz, 2H), 7.73-7.62 (m, 15H), 7.48 (t, J = 7.7 Hz, 1H), 7.26 (t, J = 7.7 Hz, 1H), 4.49 (t, J = 6.1 Hz, 2H), 3.60 (t, J = 13.6 Hz, 2H), 1.96 (m, J = 13.6, 7.2 Hz, 2H), 1.61 (m, J = 11.1 Hz, 2H). ^{13}C NMR (100 MHz, $CDCl_3$, ppm): δ 191.49, 140.71, 140.43, 135.02, 135.00, 133.55, 133.45, 131.84, 130.46, 130.34, 130.27, 129.68, 129.59, 126.51, 124.18, 122.78, 122.27, 120.39, 119.70, 118.08, 117.23, 112.45, 109.64, 109.56, 95.33, 87.28, 42.25, 29.34, 23.12, 20.13.

2.4 Synthesis of compound **3**

A mixture of KOH (2.0 g, 35.8 mmol), KI (0.4 g, 2.39 mmol) and 1,4-dibromobutane (7.73 g, 35.8 mmol) was heated to 60 ^{o}C. After reacting 1 h, 3,6-diiodocarbazole (10 g, 23.9 mmol) was added slowly, the result mixture was refluxed until TLC showed no raw material existed (about 12 h). After being cooled to room temperature, 200 mL H_2O was added, the mixture was extracted with dichloromethane (100 mL×2) . The organic phase was evaporated to give crude pruduct. The crude material was purified by column chromatography (petroleum ether:dichloromethane = 10 : 1 as the eluent) to give 6.8 g (51.4%) of **3**.

^{1}H NMR (400 MHz, $CDCl_3$, ppm): δ 8.34 (d, *J* = 1.5 Hz, 2H), 7.74 (d, *J* = 1.6 Hz, 1H), 7.71 (d, *J* = 1.6 Hz, 1H), 7.19 (s, 1H), 7.17 (s, 1H), 4.29 (t, *J* = 7.0 Hz, 2H), 3.37 (t, *J* = 6.4 Hz, 2H), 2.06-1.98 (m, 2H), 1.86 (m, *J* = 13.1, 6.5 Hz, 2H). ^{13}C NMR (100 MHz, $CDCl_3$, ppm): δ 139.38, 134.69, 129.48, 124.08, 110.76, 81.93, 42.37, 32.82, 30.02, 27.44.

2.5 Synthesis of compound **4**

A mixture of compound **3** (1 g, 1.8 mmol), 4-ethynylbenzaldehyde (0.7 g, 5.4 mmol), $Pd(PPh_3)_2Cl_2$ (5.1 mg, 0.007 mmol), CuI (2.7 mg, 0.014 mmol) and Et_3N (5 ml) was stirred at 30 ^{o}C for 12 h under the anhydrous and anaerobic conditions. the mixture was cooled to room temperature. Precipitates were filtered off and concentrated to give the crude product. The crude material was purified by column chromatography (petroleum ether:dichloromethane = 4 : 1 as the eluent) to give 0.65 g (64.5%) of **4**.

^{1}H NMR (400 MHz, $CDCl_3$, ppm): δ 10.04 (s, 2H), 8.33 (s, 2H), 7.89 (t, *J* = 7.4 Hz, 4H), 7.71 (m, *J* = 12.4, 5.8 Hz, 6H), 7.42 (d, *J* = 8.5 Hz, 2H), 4.38 (m, *J* = 12.4, 6.6 Hz, 2H), 3.42 (t, *J* = 6.3 Hz, 1H), 3.19 (t, *J* = 6.6 Hz, 1H), 2.15-2.01 (m, 2H), 1.92 (m, *J* = 13.5, 6.7 Hz, 2H). ^{13}C NMR (100 MHz, $CDCl_3$, ppm): δ 191.47, 140.67, 135.13, 133.12, 131.92, 130.18, 130.14, 129.67, 129.59, 124.63, 122.62, 113.56, 109.14, 94.83, 87.58, 32.84, 30.74, 27.59, 5.54.

2.6 Synthesis of **Mito-DCHO**

A mixture of **4** (1 g, 1.8 mmol) and acetonitrile (10 mL) was heated to 80 ^{o}C under the condition of nitrogen. After 1 h, PPh_3 (2.8 g, 10.8 mmol) was added, the result mixture was refluxed until TLC showed no raw material existed (about 36 h). After

being cooled to room temperature, the mixture was filtered and the filtrate was evaporated to give crude product. The crude product was purified through column chromatography (dichloromethane:acetonitrile = 3:1 as the eluent) to give 0.83 g (56%) of **Mito-DCHO**.

^{1}H NMR (400 MHz, DMSO-d_6, ppm): δ 10.05 (s, 2H), 8.53 (s, 2H), 7.98 (d, J = 8.0 Hz, 4H), 7.87 (m, J = 8.6, 4.6 Hz, 3H), 7.79 (d, J = 8.0 Hz, 4H), 7.76-7.68 (m, 16H), 4.51 (t, J = 6.9 Hz, 2H), 3.62 (t, J = 15.1 Hz, 2H), 2.00-1.93 (m, 2H), 1.62 (m, J = 14.1, 6.2 Hz, 2H). ^{13}C NMR (100 MHz, $CDCl_3$, ppm): δ 191.43, 140.73, 135.13, 135.08, 135.05, 133.60, 133.50, 132.15, 132.05, 131.88, 130.50, 130.37, 130.20, 130.08, 129.67, 128.57, 128.45, 124.24, 122.31, 118.10, 117.24, 113.34, 110.05, 94.88, 87.59, 42.55, 29.19, 22.66, 20.15. ESI-MS m/z: [**Mito-DCHO** - Br]$^+$ $C_{52}H_{35}NO_2P^+$ calcd, 740.2718; found, 740.2702.

3. Experimental Section

3.1. General procedures

All reagents and solvents were commercially purchased. ^{1}H-NMR spectra were recorded on Bruker-400 MHz spectrometers and ^{13}C-NMR spectra were recorded on 100 MHz spectrometers. Fluorescence spectra were obtained using a HITACHIF-2500 spectrometer. UV-vis absorption spectra were recorded on a Tech-comp UV 1000 spectrophotometer. MS spectra were conducted by ESI mass spectrometer.

The test solution of **Mito-SCHO** and **Mito-DCHO** (10 μM) in buffer solution (pH=7.4, DMSO/PBS, 1:1, v/v) was prepared. The solutions of various testing species were prepared for Cys, Hcy, GSH, Pro, Met, Val, Ala, Asp, Trp, Tyr, Ile, His, Thr, Ser, Hyp, Leu, Phe, SCN^-, S^{2-}, SO_4^{2-}, $S_2O_3^{2-}$, SO_3^{2-}, CH_3COO^-,

Cl^-, CO_3^{2-}, NO_3^-, NO_2^-, Cu^{2+}, Na^+, Mg^{2+} and Fe^{3+}. Various ROS including H_2O_2, ClO^-, $O_2^{\bullet-}$, TBHP, $HO\cdot$, *t*-$BuO\cdot$ and CH_3COOOH were prepared according to the procedure reported previously.[3] The resulting solution was shaken well and incubated for 20 min at room temperature before recording the spectra.

3.2. Measurement of two-photon absorption cross-section (δ)

Two-photon excitation fluorescence (TPEF) spectra were measured using femtosecond laser pulse and Ti: sapphire system (680~1080 nm, 80 MHz, 140 fs, Chameleon II) as the light source. All measurements were carried out in air at room temperature. Two-photon absorption cross-sections were measured using two-photon-induced fluorescence measurement technique. The two-photon absorption cross-sections (δ) were determined in DMSO with **Mito-DCHO/Mito-DCHO** (0.1 mM) with the addition of Cys (0.6 mM) by using optically matching solutions of fluorescein as a standard, according to the following equation:

$$\delta = \delta_{ref} \frac{\Phi_{ref}}{\Phi} \frac{c_{ref}}{c} \frac{n_{ref}}{n} \frac{F}{F_{ref}}$$

Here, the subscripts ref stands for the reference molecule. δ is the TPA cross-section value, c is the concentration of solution, n is the refractive index of the solution, F is the TPEF integral intensities of the solution emitted at the exciting wavelength, and Φ is the fluorescence quantum yield. The Φ_{ref} value of reference ($\Phi_{fluorescein}$ = 0.97) is taken from the literature.[4] The δ_{ref} value of reference was taken from the literature,[5] and the relative error of δ value in the experiment is about ±15%.

3.3. Cytotoxicity assay

MTT (5-dimethylthiazol-2-yl-2, 5-diphenyltetrazolium bromide) assay was performed as previously reported to test the cytotoxic effect of the probe in cells.[6] HeLa cells were passed and plated to ca. 70% confluence in 96-well Plates 24 h before treatment. Prior to **Mito-DCHO** treatment, DMEM (Dulbecco's Modified Eagle Medium) with 10% FCS (Fetal Calf Serum) was removed and replaced with fresh DMEM, and aliquots of **Mito-DCHO** stock solutions (1 mM DMSO) were added to obtain final concentrations of 10, 20 and 30mM respectively. The treated cells were incubated for 24 h at 37°C under 5%CO_2. Subsequently, cells were treated with 5 mg/mL MTT (40 mL/well) and incubated for an additional 4 h (37 °C, 5% CO_2). Then the cells were dissolved in DMSO (150 mL/well), and the absorbance at 570 nm was recorded. The cell viability (%) was calculated according to the following equation:

Cell viability % = OD_{570} (sample)/OD_{570} (control) × 100 %

where OD_{570}(sample) represents the optical density of the wells treated with various concentration of **Mito-DCHO** and OD_{570}(control) represents that of the wells treated with DMEM containing 10% FCS. The percent of cell survival values is relative to untreated control cells.

3.4. Cell culture and two-photon fluorescence microscopy imaging

For two-photon imaging, HeLa cells were cultured in DMEM supplemented with 10% FCS, penicillin (100 μg/mL), and streptomycin (100 μg/mL) at 37°C in a humidified atmosphere with 5% CO_2 and 95% air. Cytotoxicity assays show that **Mito-DCHO** is safe enough for two-photon bio-imaging at low concentrations. The cells were first washed with PBS, incubated with probe,

N-ethylmaleimide (NEM), thiol and H_2O_2 respectively in the incubator at 37 °C and then rinsed for three times with PBS. Cells imaging was carried out on a confocal microscope (Zeiss LSM 510 Meta NLO). Two-photon fluorescence microscopy images of labeled cells were obtained by exciting the probe with a mode-locked titanium–sapphire laser source at 720 nm.

3.5. Dual-color imaging of mitochondrial oxidative stress levels under LPS-induced apoptosis

TPM images of mitochondrial oxidative stress levels under LPS-induced apoptosis utilizing probe **Mito-DCHO**. Cells were incubated with **Mito-DCHO** (10 μM) for 30 min, and imaged. Cells were mediated by LPS (5 μg/mL) for 0.5, 1.0, 1.5, 2.0 and 2.5 h, respectively, subsequently incubated with **Mito-DCHO** (10 μM) for 30 min and imaged. Cells imaging was carried out on a confocal microscope (Zeiss LSM 510 Meta NLO). Two-photon fluorescence microscopy images of labeled cells were obtained by exciting the probe with a mode-locked titanium–sapphire laser source at 720 nm.

3.6. Ratiometric TPM images in zebrafish during LPS-induced apoptosis

All procedures involving animals were approved by and conformed to the guidelines of the Anhui University Animal Care Committee, School of life science. We have taken great efforts to reduce the number of animal used in these studies and also taken effort to reduce animal suffering from pain and discomfort.

Ratiometric TPM images in zebrafish during LPS-induced apoptosis. Zebrafishes were mediated by LPS (100 μg/mL) for 0, 0.5, 1, 1.5 and 2 h, respectively, subsequently incubated with **Mito-DCHO** (20 μM) for 0.5 h. All

the fishes were terminally anaesthetized using MS222, and images were carried out on a confocal microscope (Zeiss LSM 710 Meta NLO). Two-photon fluorescence microscopy images of zebrafishes were obtained by exciting **Mito-DCHO** with a mode-locked titanium–sapphire laser source at 720 nm.

References

(1) L. J. Goerigk, J. Chem. *Theory Comput.*, 2014, **10**, 968-980.

(2) Y. Zhao and D. G.Truhlar, *Theor. Chem. Acc.*, 2008, **120**, 215-241.

(3) (a) L. Yuan, L. Wang, B. K. Agrawalla, S. J. Park, H. Zhu, B. Sivaraman, J. Peng, Q. H. Xu, Y. T. Chang, *J. Am. Chem. Soc.*, 2015, **137**, 5930-5938. (b) M. S. Chan, D. Xu, L. Guo, D. Y. Tam, L. S. Liu, Y. Chen, M. S. Wong, P. K. Lo, *Org. Biomol. Chem.*, 2015, **13**, 7307-7312. (c) X.T. Jia, Q.Q. Chen, Y.F. Yang, Y. Tang, R. Wang, Y.F. Xu, W.P. Zhu, X.H. Qian, *J. Am. Chem. Soc.,* 2016, **138**, 10778-10781. (d) W. Zhang, X. Wang, P. Li, H. Xiao, W. Zhang, H. Wang, B. Tang, *Anal. Chem.,* 2017*,* **89***,* 6840-6845. (e) M. R. Clinea, J. P. Toscano, *J. Phys. Org. Chem.,* 2011, **24**, 993-998.

(4) G. A. Crosby, J. N. Demas, J. Phys. Chem., 1971, **75**, 991-1024.

(5) N. S. Makarov, M. Drobizhev, A. Rebane, *Opt. Express,* 2008, **16**, 4029-4047.

(6) D. F. Yao, Z. Lin, J. C. Wu, *ACS Appl. Mater. Inter.,* 2016, **8**, 5847-5856.

4. Time-dependent fluorescent response of **Mito-SCHO** to Cys

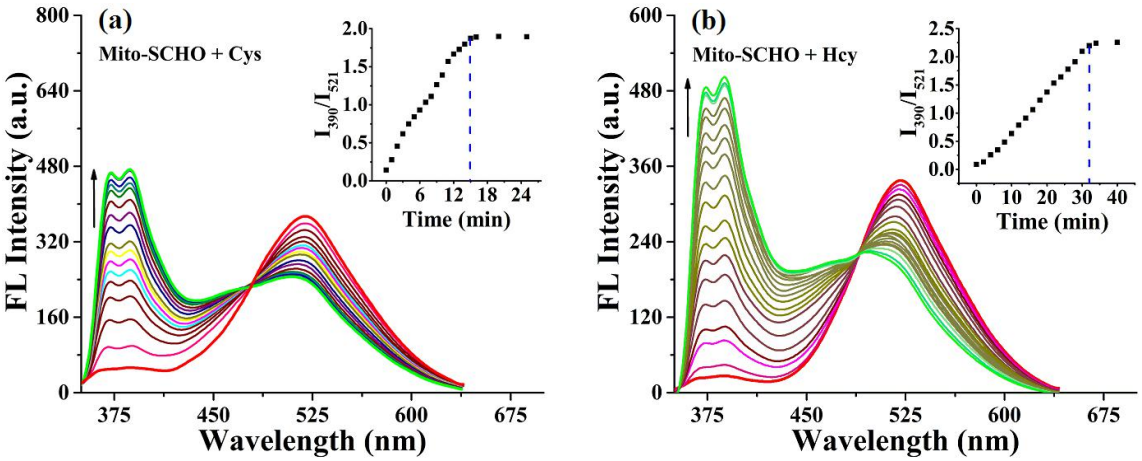

Fig. S3 Time-dependent fluorescence spectra response of **Mito-SCHO** (10 μM, λ_{ex} = 345 nm) with (a) Cys (60 μM) and (b) Hcy (60 μM) in PBS/DMSO (5:5, v/v, pH=7.4). Inset: Relationships between time and the emission ratio (I_{390nm}/I_{521nm}) changes of **Mito-SCHO** towards Cys (a) and Hcy (b).

5. Time-dependent UV-vis spectra of **Mito-SCHO** and **Mito-DCHO** to Cys/Hcy

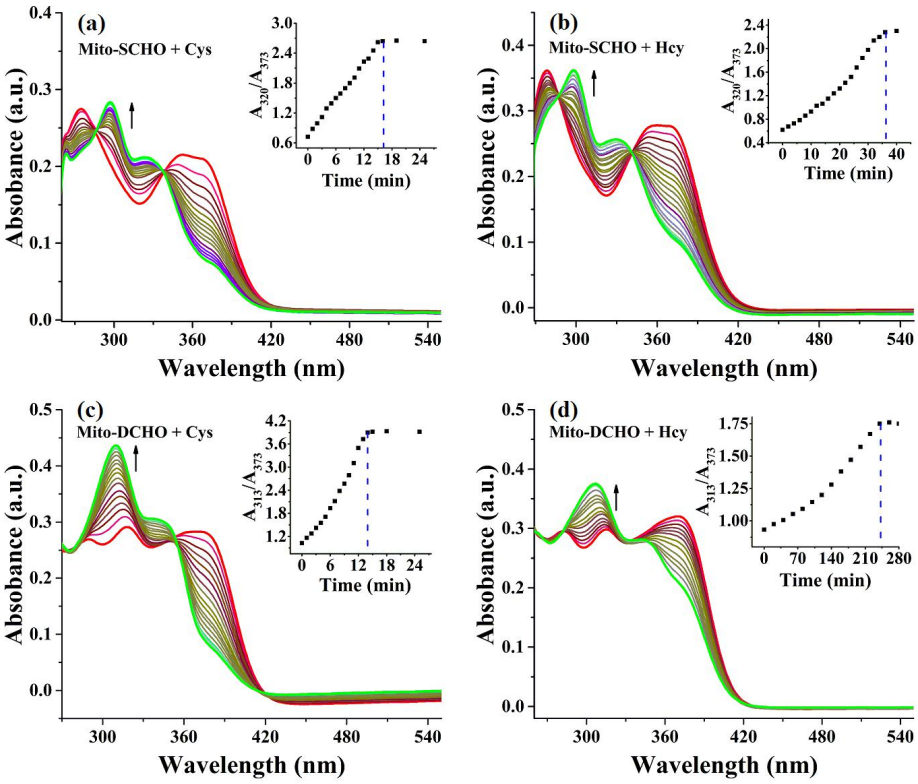

Fig. S4 Time-dependent UV-vis absorption response of (a) **Mito-SCHO** (10 μM) with Cys (60

μM), (b) **Mito-SCHO** (10 μM) with Hcy (60 μM), (c) **Mito-DCHO** (10 μM) with Cys (60 μM), (d) **Mito-DCHO** (10 μM) with Hcy (60 μM) in PBS/DMSO (5:5, v/v, pH=7.4). Inset: Relationships between time and the absorbance ratio (A_{320nm}/A_{373nm}) changes of (a) **Mito-SCHO** with Cys, (b) **Mito-SCHO** with Hcy; Relationships between time and the absorbance ratio (A_{313nm}/A_{373nm}) changes of (c) **Mito-DCHO** with Cys, (d) **Mito-DCHO** with Hcy.

6. Chemical stability and competitive experiment

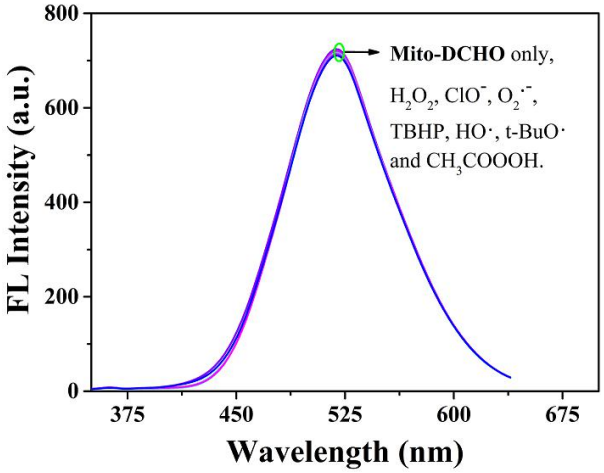

Fig. S5 Fluorescence spectra of **Mito-DCHO** (10 μM) upon addition of various ROS (60 μM, including H_2O_2, ClO^-, $O_2^{\bullet-}$, TBHP, $HO\cdot$, *t*-$BuO\cdot$ and CH_3COOOH) in PBS/DMSO buffer solution (5:5, v/v, pH=7.4, λ_{ex} = 345 nm).

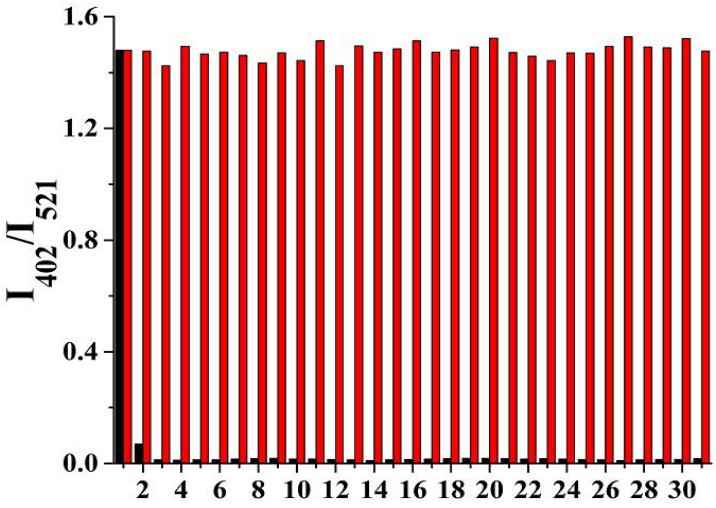

Fig. S6 Emission ratios (I_{402nm}/I_{521nm}) of **Mito-DCHO (**10 μM**)** upon addition of analytes (60 μM)

in PBS/DMSO buffer solution (5:5, v/v, pH=7.4, λ_{ex} = 345 nm). Black and red bars represent the fluorescence ratio of probe in the presence of various analytes before and after addition of Cys, respectively. Each spectrum was acquired 20 min after addition of various analytes. 1, Cys; 2, Hcy; 3, GSH; 4, Pro; 5, Met; 6, Val; 7, Ala; 8, Asp; 9, Trp; 10, Tyr; 11, Ile; 12, His; 13, Thr; 14, Ser; 15, Hyp; 16, Leu; 17, Phe; 18, SCN^-; 19, S^{2-}; 20, $SO4^{2-}$; 21, $S_2O_3^{2-}$; 22, SO_3^{2-}; 23, CH_3COO^-; 24, Cl^-; 25, CO_3^{2-}; 26, NO_3^-; 27, NO_2^-; 28, Cu^{2+}; 29, Na^+; 30, Mg^{2+}; 31, Fe^{3+}.

7. Fluorescence and UV-vis absorption spectra of **Mito-DCHO** to Cys concentrations

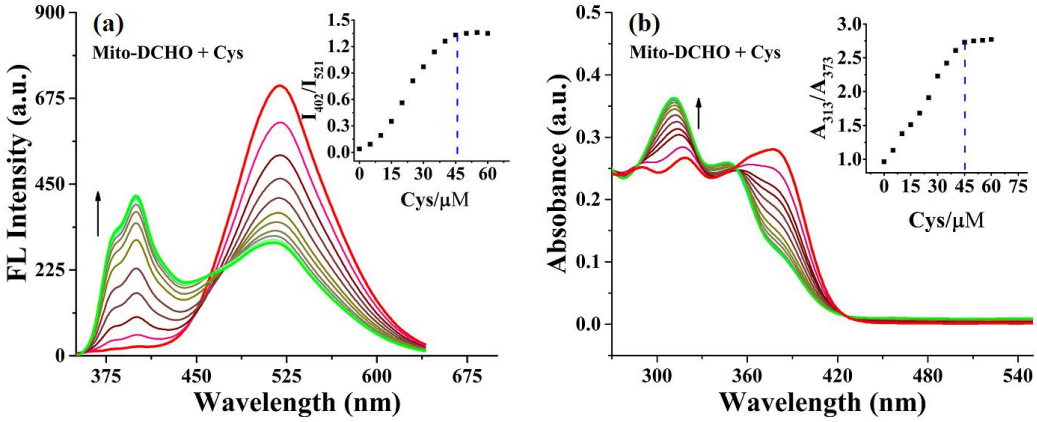

Fig. S7 Fluorescence spectra (a) and UV-vis absorption spectra (b) of **Mito-DCHO** (10 μM) in the presence of increasing amount of Cys (0~60 μM) in PBS/DMSO (5:5, v/v, pH=7.4, λ_{ex} = 345 nm). Inset: Relationship between the emission ratio (I_{402nm}/I_{521nm}) changes of **Mito-DCHO** (a) with Cys, and the relationship between the absorbance ratio (A_{313nm}/A_{373nm}) changes of **Mito-DCHO** (b) with Cys concentrations. Spectra were recorded for 20 min after Cys addition.

8. Determination of detection limit

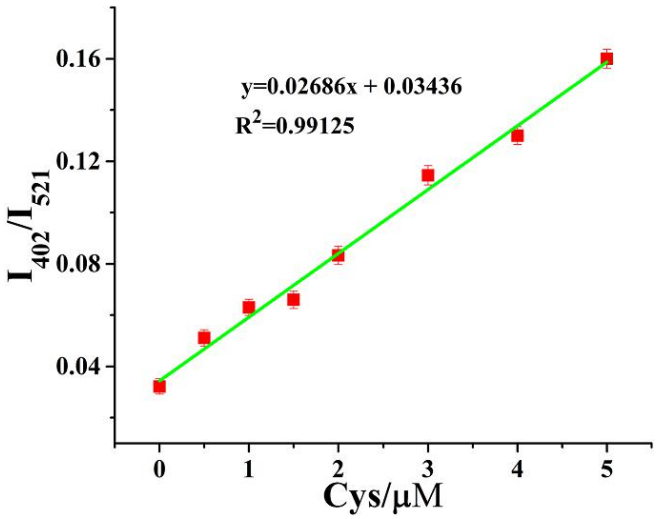

Fig. S8 Emission ratio (I_{402nm}/I_{521nm}) changes of **Mito-DCHO** (10 μM) upon addition of Cys (0~5 μM) in PBS/DMSO (5:5, v/v, pH=7.4, λ_{ex} = 345 nm).

9. Determination of pH effect

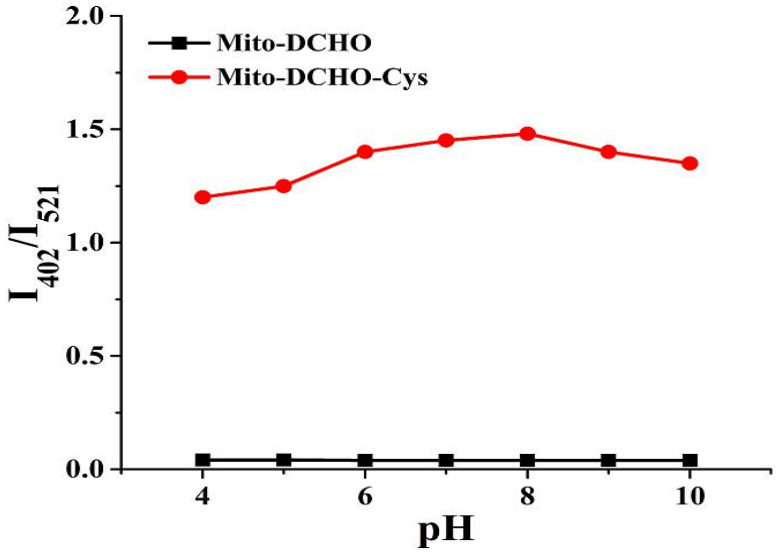

Fig. S9 Emission ratio (I_{402nm}/I_{521nm}) of **Mito-DCHO (**10 μM**)** at various pH values in the absence (black) and presence (red) of Cys (60 μM) in PBS/DMSO buffer (5/5, v/v, pH=7.4, λ_{ex} = 345 nm) . Each spectrum was recorded after 20 min.

10. ^{1}H-NMR titration

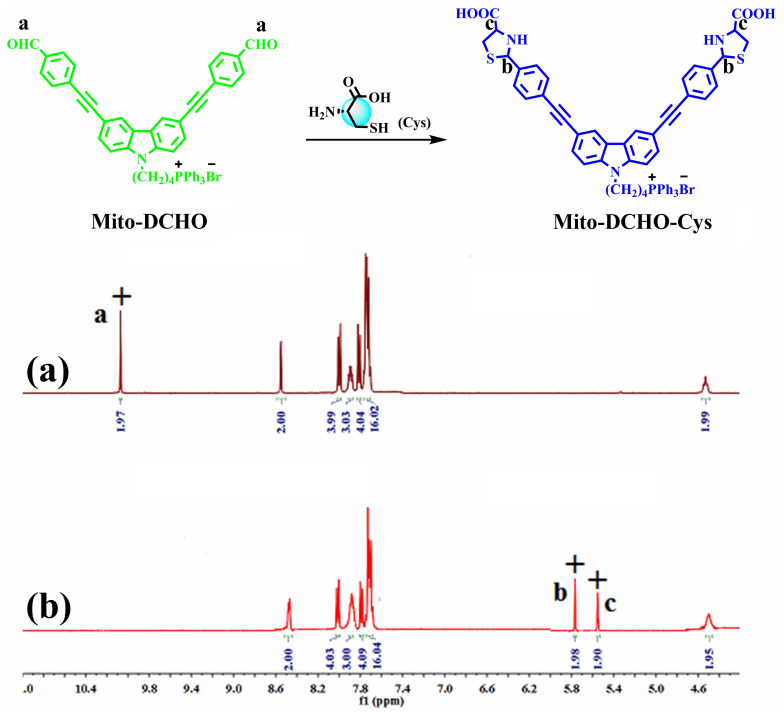

Fig. S10 ^{1}H NMR spectra of (a) **Mito-DCHO** and (b) **Mito-DCHO-Cys** in DMSO-d_6.

11. ESI-MS spectra of **Mito-DCHO**, **Mito-DCHO**-Cys, **Mito-SCHO** and **Mito-SCHO**-Cys/Hcy

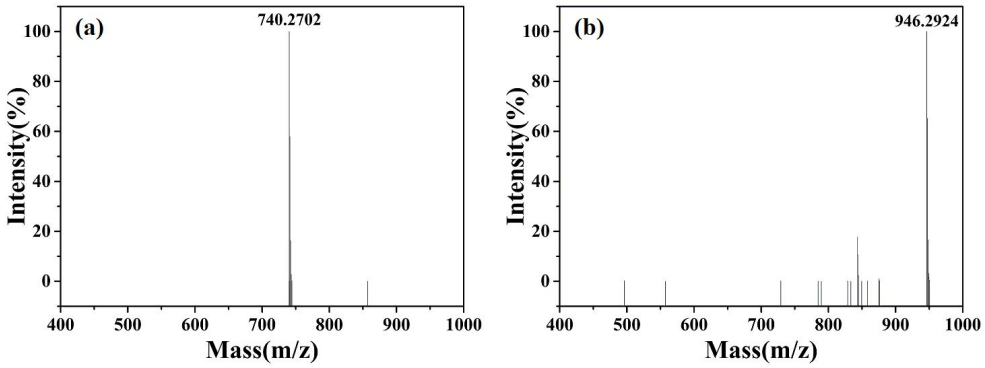

Fig. S11 (a) ESI-MS spectrum of **Mito-DCHO**. (ESI-MS m/z: [**Mito-DCHO** - Br]$^{+}$ $C_{52}H_{35}NO_2P^{+}$ calcd, 740.2718; found, 740.2702.) (b) ESI-MS spectrum of **Mito-DCHO**-Cys. (ESI-MS m/z: [**Mito-DCHO**-Cys - Br]$^{+}$ $C_{58}H_{49}N_3O_4S_2P^{+}$ calcd, 946.2902; found, 946.2924.)

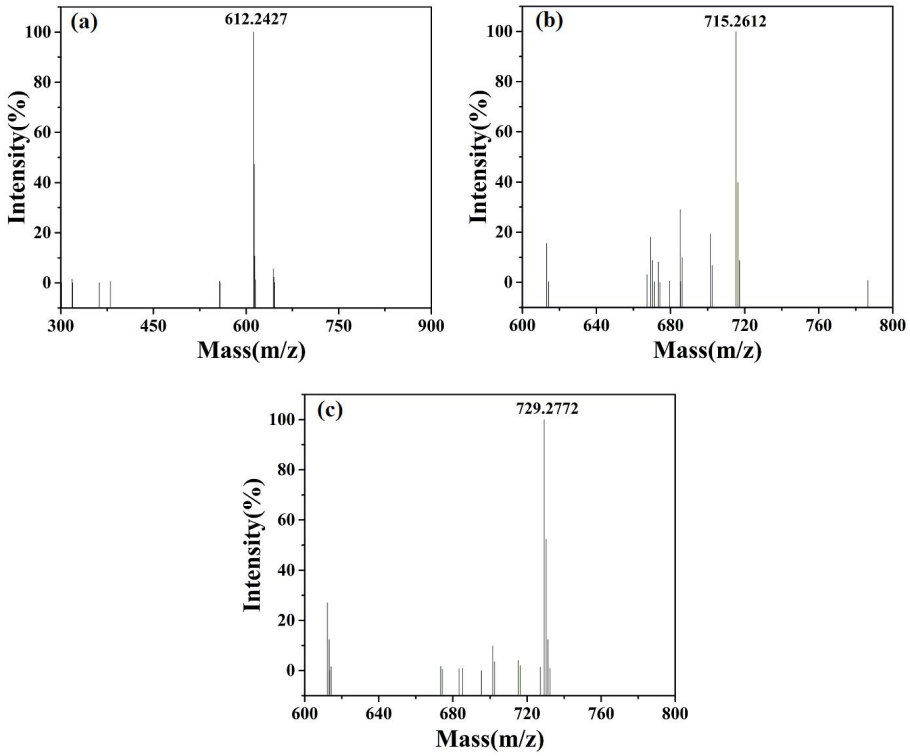

Fig. S12 (a) ESI-MS spectrum of **Mito-SCHO**. (ESI-MS m/z: [**Mito-SCHO** - Br]$^+$ $C_{43}H_{35}NOP^+$ calcd, 612.2456; found, 612.2427.) (b) ESI-MS spectrum of **Mito-SCHO**-Cys. (ESI-MS m/z: [**Mito-SCHO-Cys** - Br]$^+$ $C_{46}H_{40}N_2O_2SP^+$ calcd, 715.2548; found, 715.2612.) (c) ESI-MS spectrum of **Mito-SCHO**-Hcy. (ESI-MS m/z: [**Mito-SCHO-Hcy** - Br]$^+$ $C_{47}H_{42}N_2O_2SP^+$ calcd, 729.2705; found, 729.2772.)

12. Two-photon absorption properties

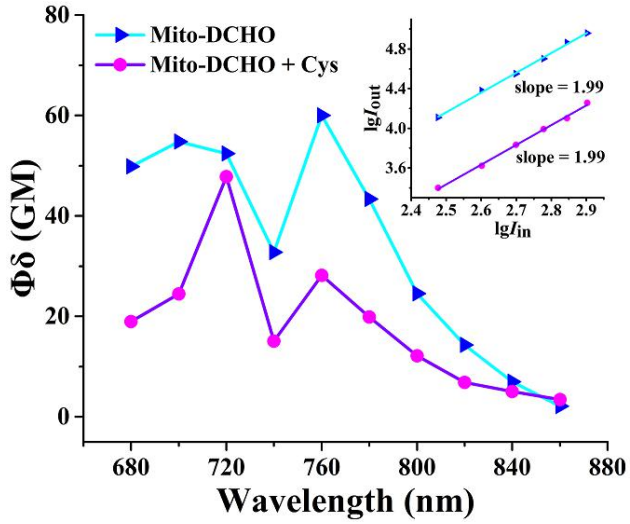

Fig. S13 Two-photon absorption cross-section values of **Mito-DCHO** (0.1mM) and

Mito-DCHO (0.1mM) with the addition of Cys (0.6 mM). Inset: The square relationship of two-photon excited fluorescence intensity (I_{out}) of **Mito-DCHO** and **Mito-DCHO** + Cys with input power (I_{in} = 300-800 mW). Excitation was carried out at 760 nm and 720 nm, respectively.

13. Cytotoxicity Assays

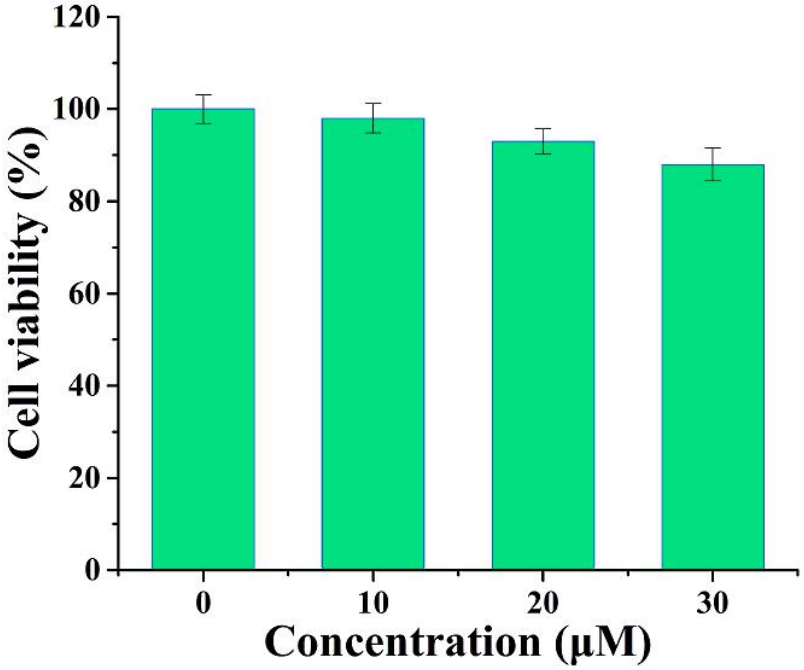

Fig. S14 Cytotoxicity data of **Mito-DCHO** (Hela cells incubated for 24 h).

14. TPM imaging of **Mito-DCHO**'s mitochondria-targeted capability

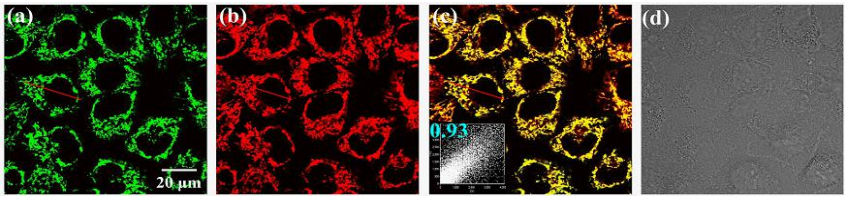

Fig. S15 TPM images of **Mito-DCHO**'s mitochondrial location. HeLa cells were co-stained with **Mito-DCHO** (10 μM) and Mitotracker red (1 μM) for 30 min at 37 ˚C. From left to right: (a) λ_{em} = 500−540 nm (**Mito-DCHO**, λ_{ex} =720 nm) (b) λ_{em} =580-600 nm (Mitotracker red, λ_{ex} = 579 nm) (c) Merge, overlay of of (a) and (b). Insert: Intensity scatter plot of green and red channels. (d) Bright Field. Scale bar: 20 μm.

15. Dual-color imaging of **Mito-DCHO** to exogenous and endogenous Cys in cells

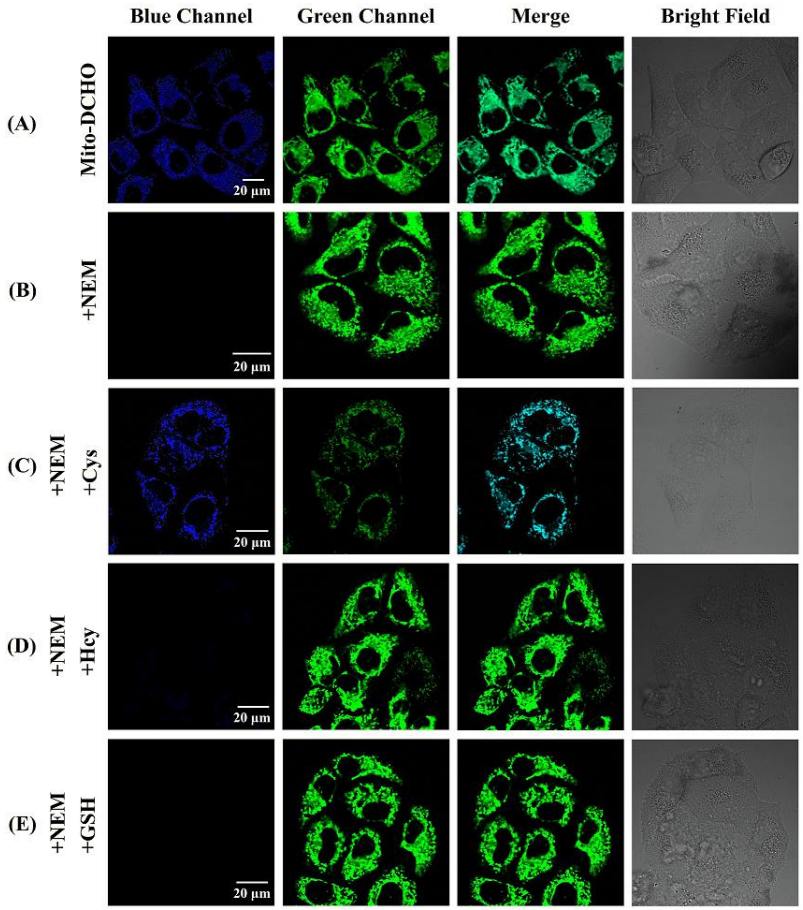

Fig. S16 Dual-color images of **Mito-DCHO** responding to mitochondrial Cys in living HeLa cells. (A) HeLa cells were incubated with **Mito-DCHO** (10 μM) for 30 min. (B, C, D, E) HeLa cells were pretreated with NEM (1.0 mM) for 30 min and then incubated with blank, Cys, Hcy and GSH (60 μM) for 1 h, respectively, and finally incubated with **Mito-DCHO** (10μM) for 30 min. From left to right: Blue Channel: λ_{em} = 420-460 nm, Green Channel: λ_{em} = 500-540 nm, Merge and Bright Field. λ_{ex} = 720 nm. Scale bar: 20 μm.

16. Dual-color imaging of mitochondrial Cys under oxidative stress induced by H_2O_2

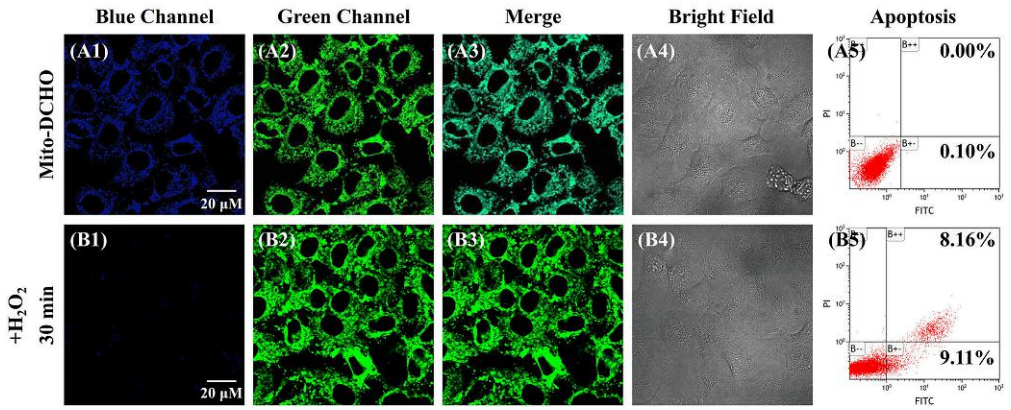

Fig. S17 TPM images of **Mito-DCHO** in the absence and presence of H_2O_2 in living HeLa cells (1-4) and apoptosis analysis (5). (1-4) Cells were mediated by H_2O_2 (200 μM) for 0 and 30 min (A-B) respectively, subsequently incubated with **Mito-DCHO** (10 μM, 30 min), and imaged. From left to right: Blue Channel: λ_{em} = 420−460 nm, Green Channel: λ_{em} = 500−540 nm, Merge, Bright Field and Apoptosis. λ_{ex} = 720 nm. Scale bar: 20 μm. (5) HeLa Cells were mediated by H_2O_2 (200 μM) for 0 and 30 min (A5-B5) respectively, then cells were harvested and the percentage of cell apoptosis was analyzed by flow cytometer *via* Annexin V-FITC/PI Apoptosis Detection Kit. Apoptosis analysis: areas of B－＋, B＋＋, B－－, B＋－ were corresponding necrotic, late apoptosis, viable, and early apoptosis.

17. Dual-color imaging of mitochondrial oxidative stress levels under LPS-induced apoptosis

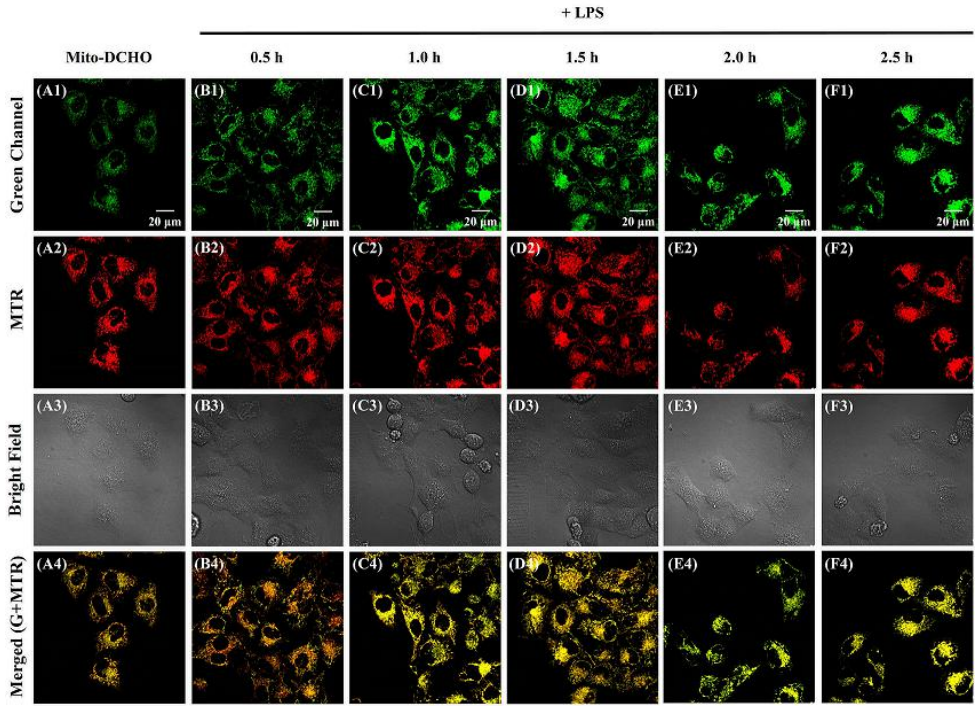

Fig. S18 TPM images of mitochondrial oxidative stress levels under LPS-induced apoptosis utilizing probe **Mito-DCHO**. (A) Cells were incubated with **Mito-DCHO** (10 μM) for 30 min, and imaged. (B-F) Cells were mediated by LPS (5 μg/mL) for 0.5, 1.0, 1.5, 2.0 and 2.5 h respectively, subsequently incubated with **Mito-DCHO** (10 μM) for 30 min and imaged. From top to bottom: Green Channel: λ_{em} = 500-540 nm, λ_{ex} = 720 nm ; MTR: λ_{em} =580-600 nm (Mitotracker red, λ_{ex} = 579 nm), Bright Field, Merge: overlay of Green Channel and MTR. Scale bar: 20 μm.

18. Ratiometric TPM images in zebrafish during LPS-induced apoptosis

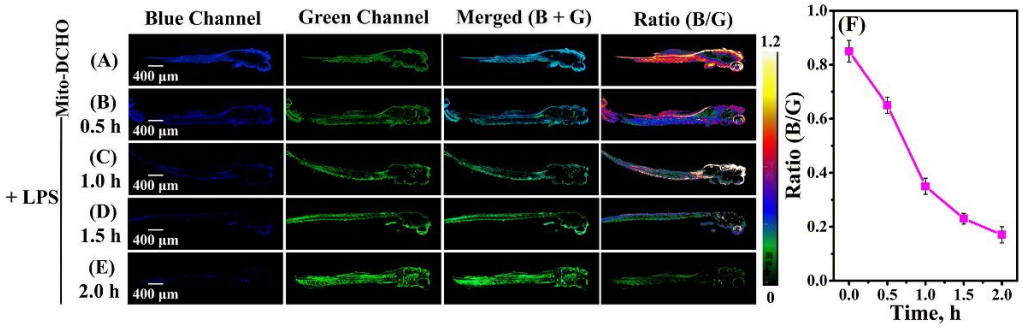

Fig. S19 Ratiometric TPM images in zebrafish during LPS-induced apoptosis. (A-E) Zebrafishes were mediated by LPS (100 μg/mL) for 0, 0.5, 1, 1.5 and 2 h respectively, subsequently incubated with **Mito-DCHO** (20 μM) for 0.5 h, and imaged. From left to right: Blue Channel: λ_{em} = 420-460 nm; Green Channel: λ_{em} = 500-540 nm, λ_{ex} = 720 nm; Merge and ratio imaging of blue/green channel. Scale bar: 400 μm. (F) Fluorescence intensity ratios (I_{blue}/I_{green}) values in panels A-E. Data are expressed as mean ±SD of three parallel experiments.

19. NMR Spectra and mass original spectra

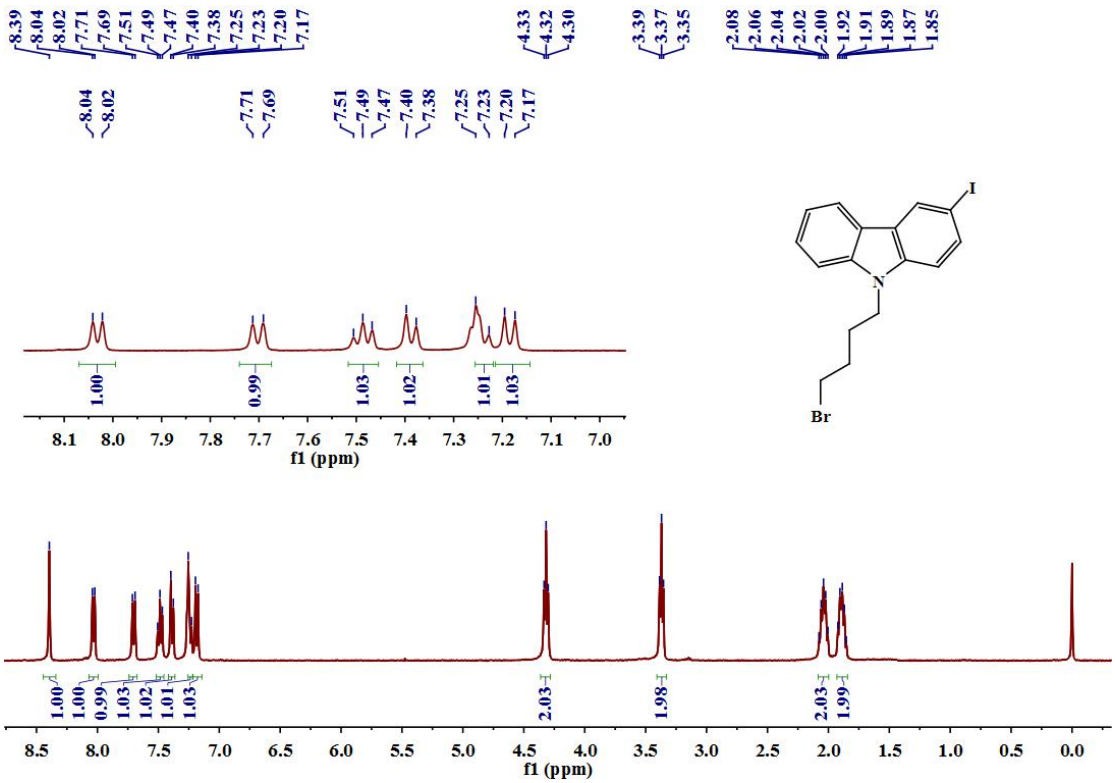

Fig. S20 ^{1}H NMR spectra of compound **1** in $CDCl_3$.

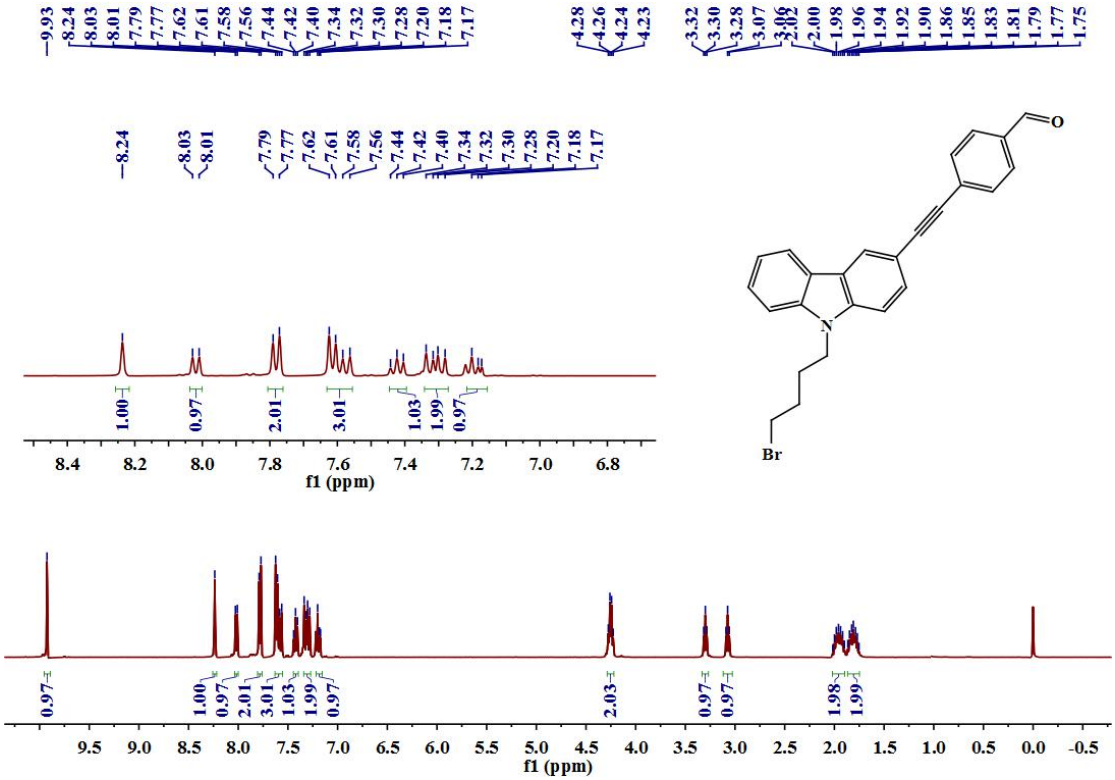

Fig. S21 ^{1}H NMR spectra of compound **2** in $CDCl_3$.

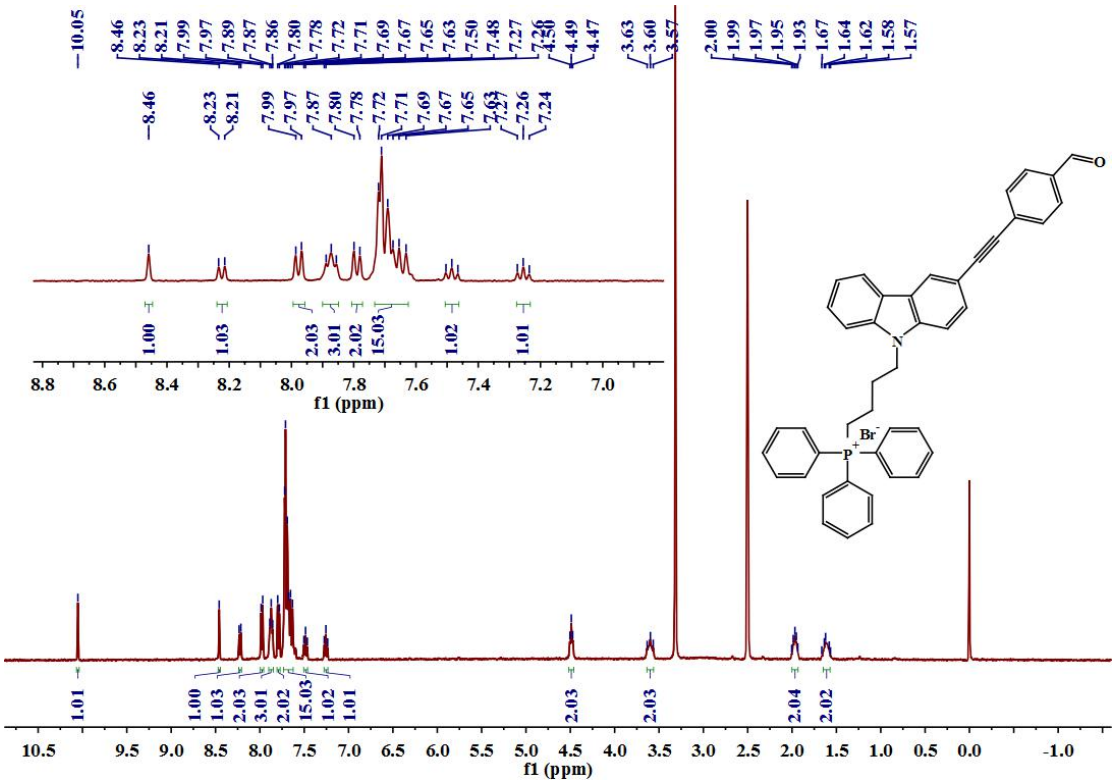

Fig. S22 ^{1}H NMR spectra of compound **Mito-SCHO** in DMSO-d_6.

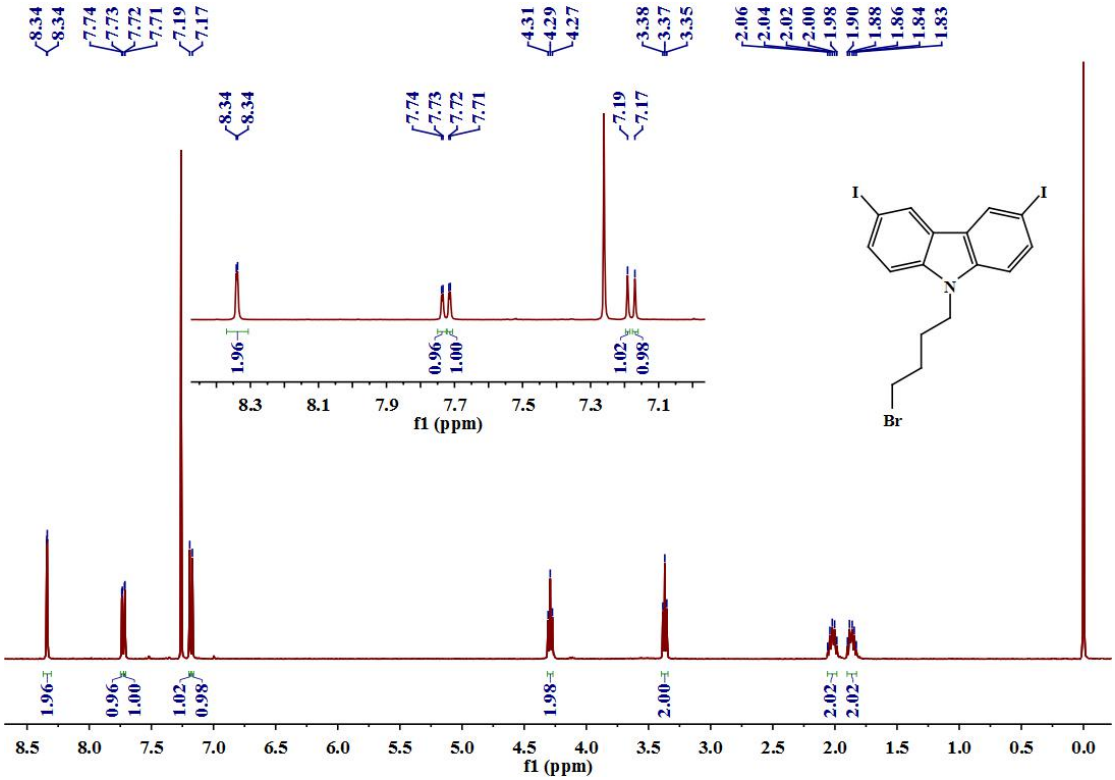

Fig. S23 ^{1}H NMR spectra of compound **3** in $CDCl_3$.

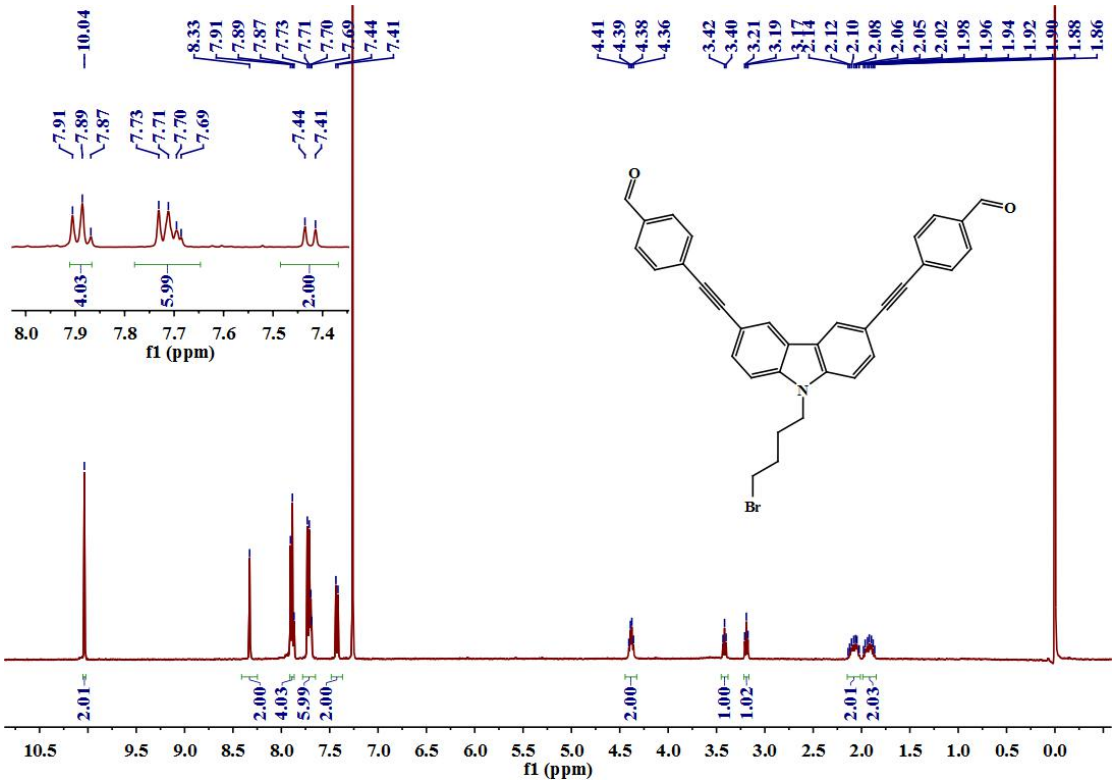

Fig. S24 ^{1}H NMR spectra of compound **4** in $CDCl_3$.

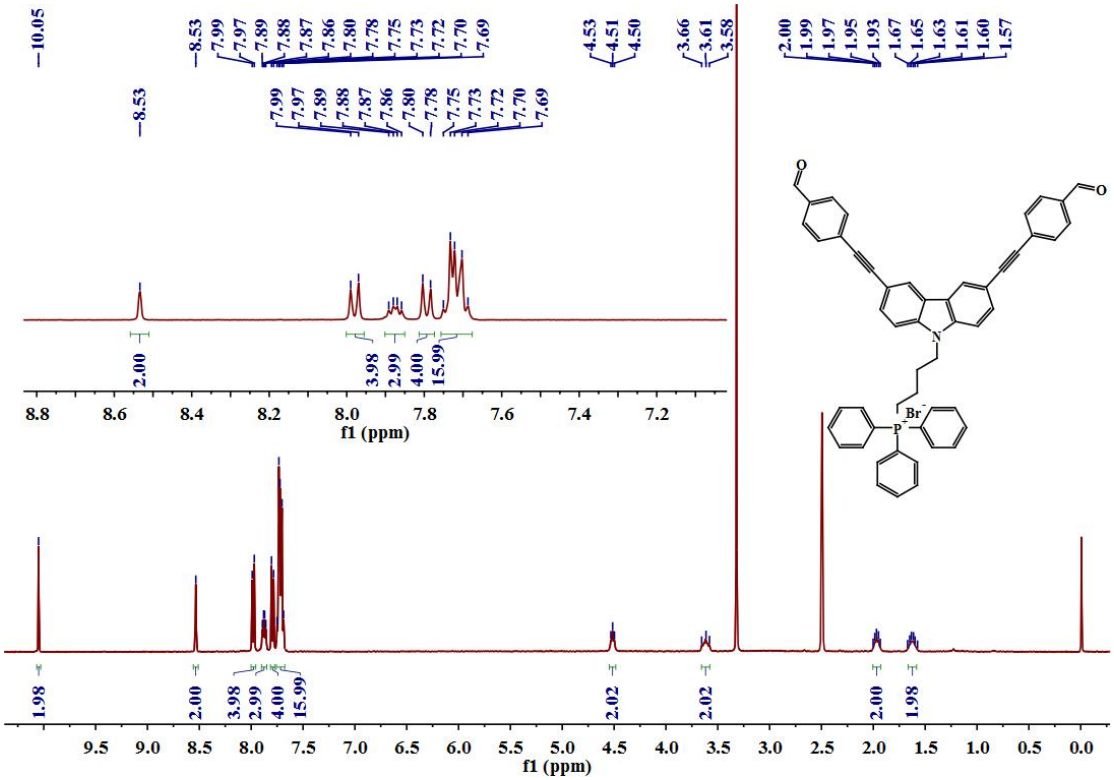

Fig. S25 ^{1}H NMR spectra of **Mito-DCHO** in DMSO-d_6.

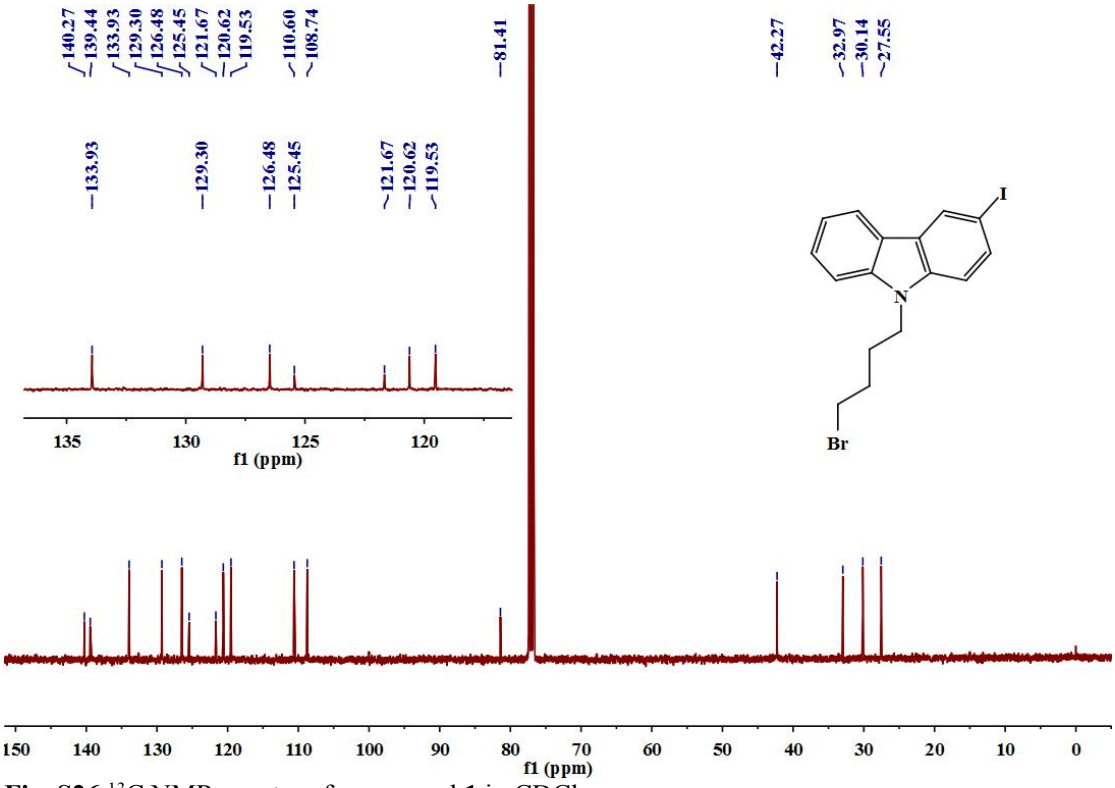

Fig. S26 ^{13}C NMR spectra of compound **1** in $CDCl_3$.

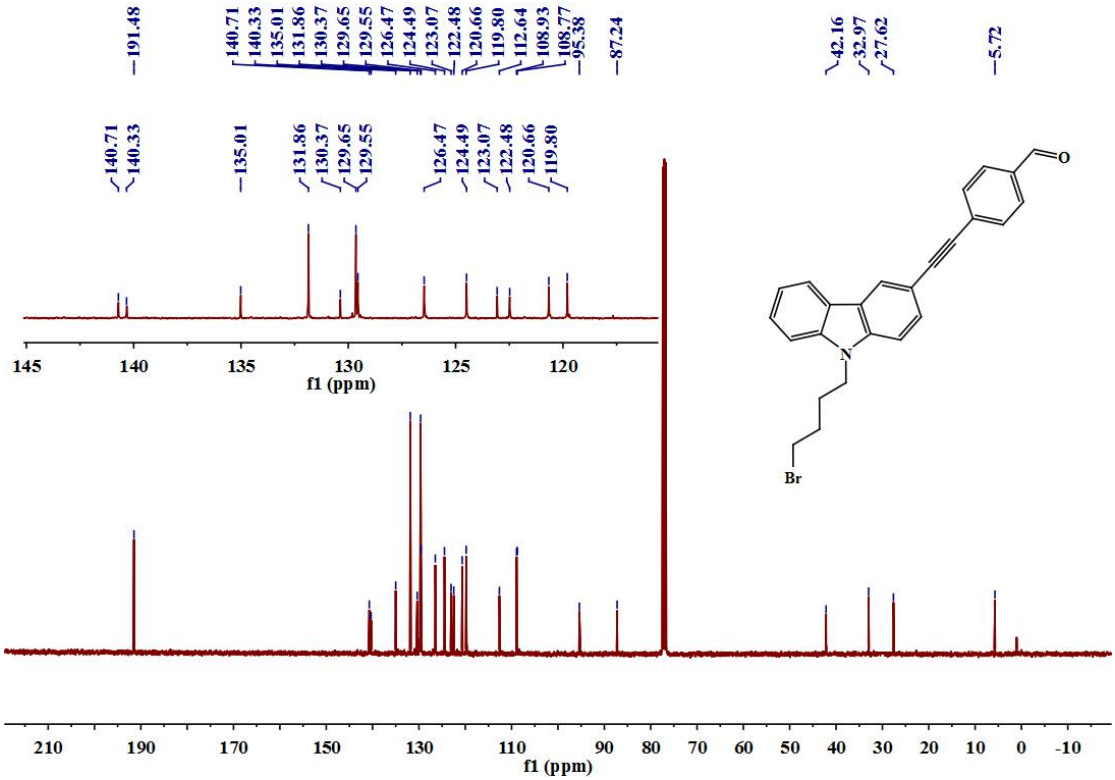

Fig. S27 ^{13}C NMR spectra of compound **2** in $CDCl_3$.

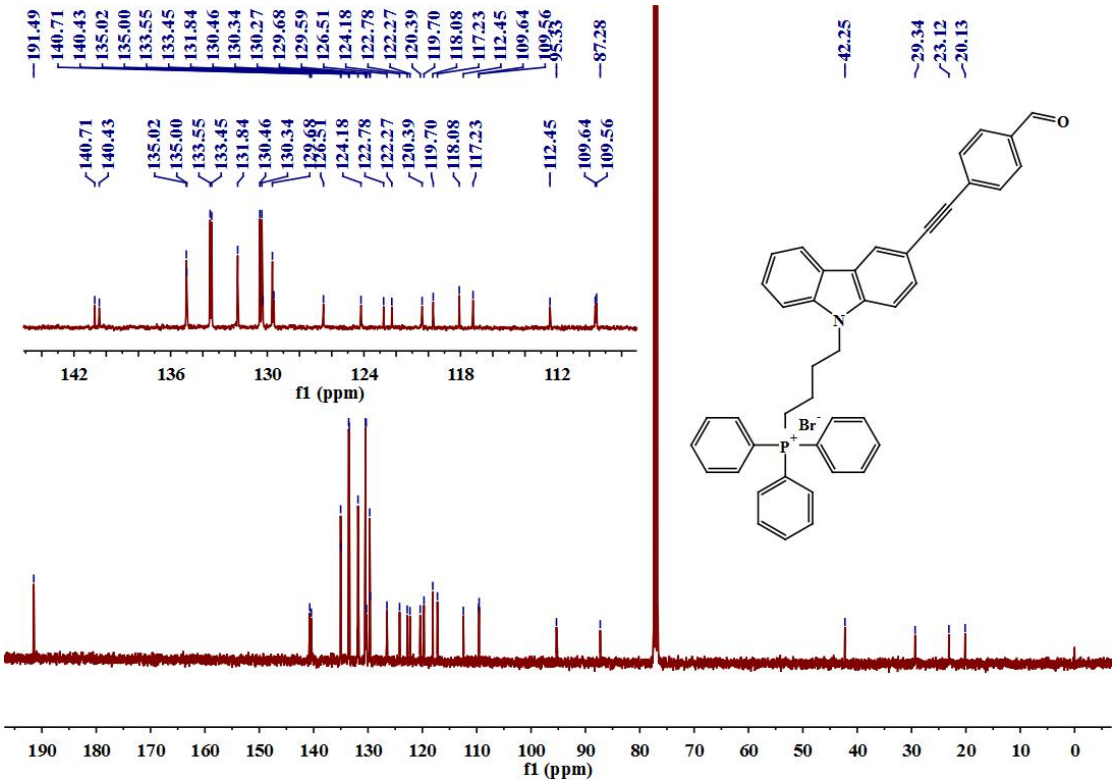

Fig. S28 ^{13}C NMR spectra of compound **Mito-SCHO** in DMSO-d_6.

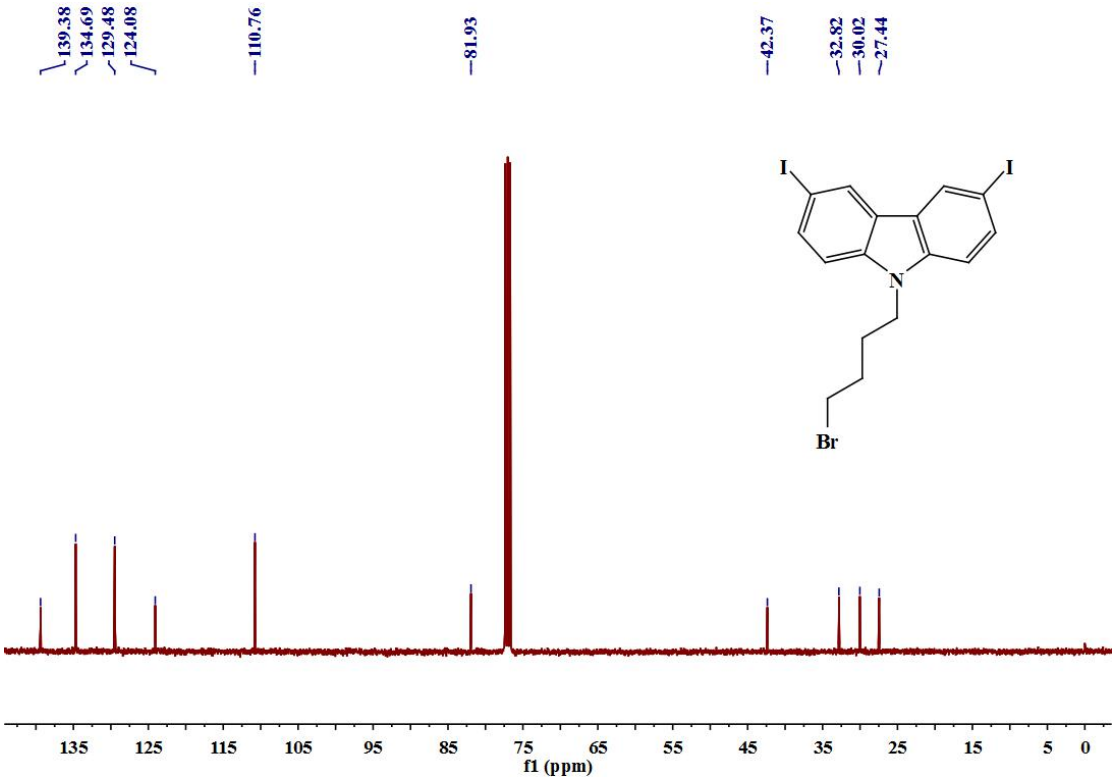

Fig. S29 ^{13}C NMR spectra of **3** in $CDCl_3$.

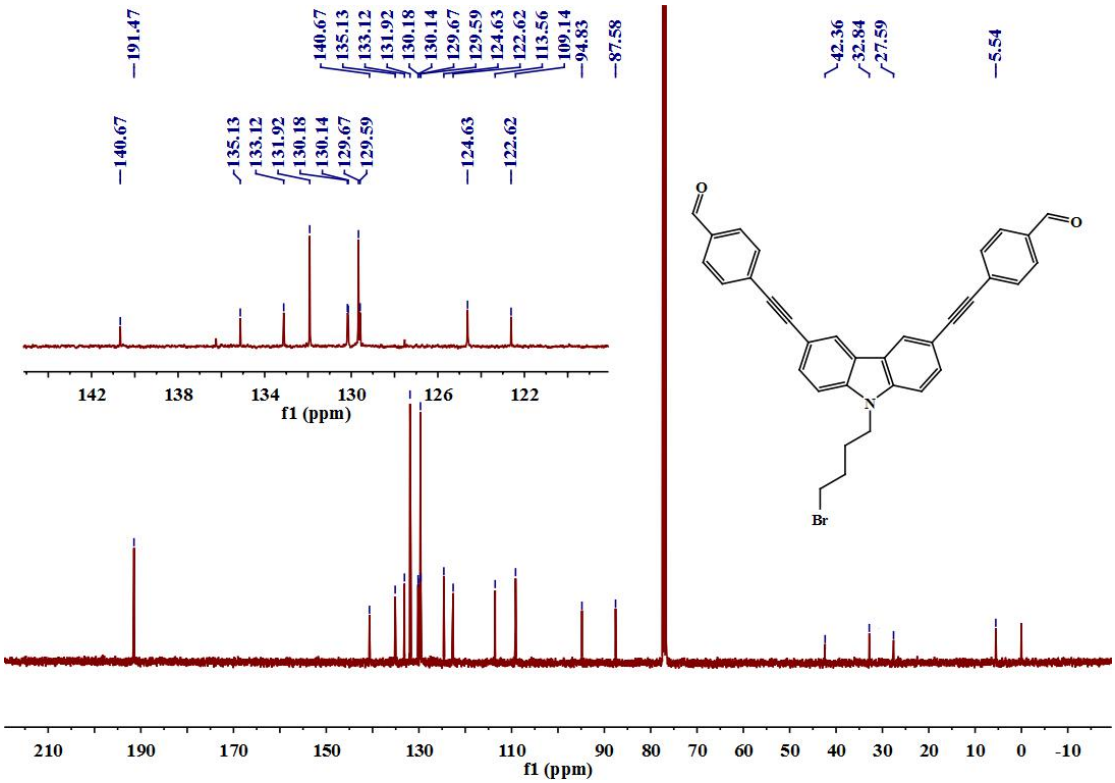

Fig. S30 ^{13}C NMR spectra of compound **4** in $CDCl_3$.

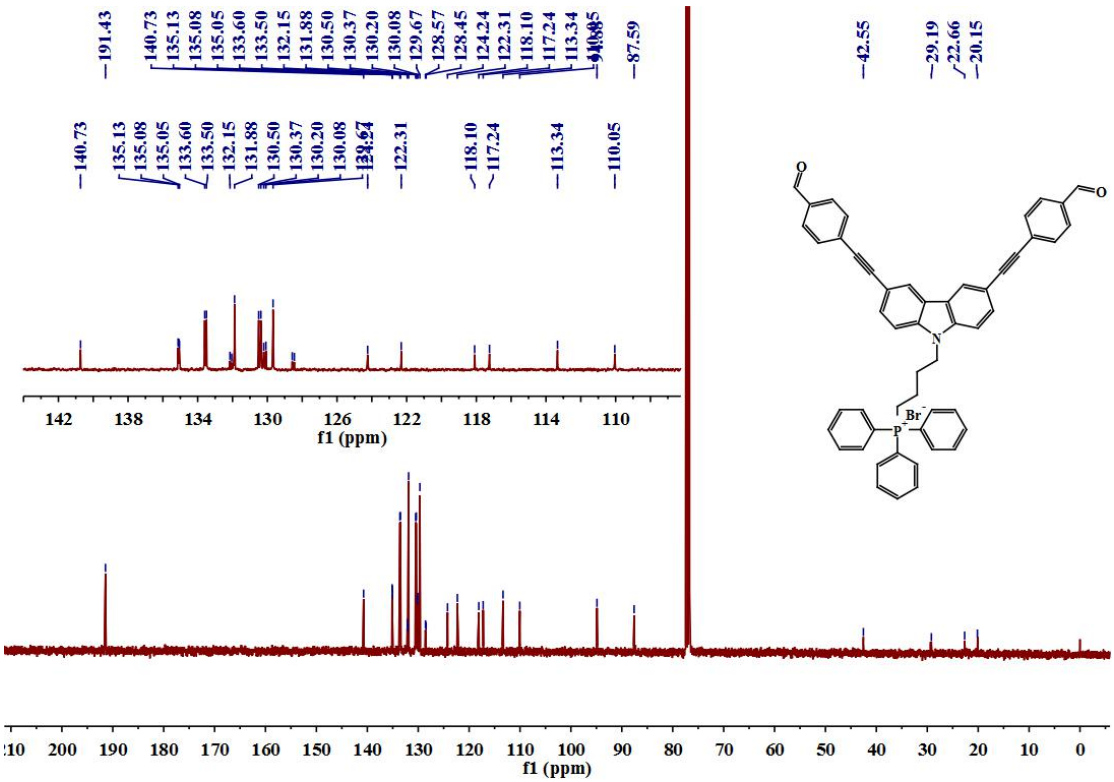

Fig. S31 ^{13}C NMR spectra of **Mito-DCHO** in DMSO-d_6.

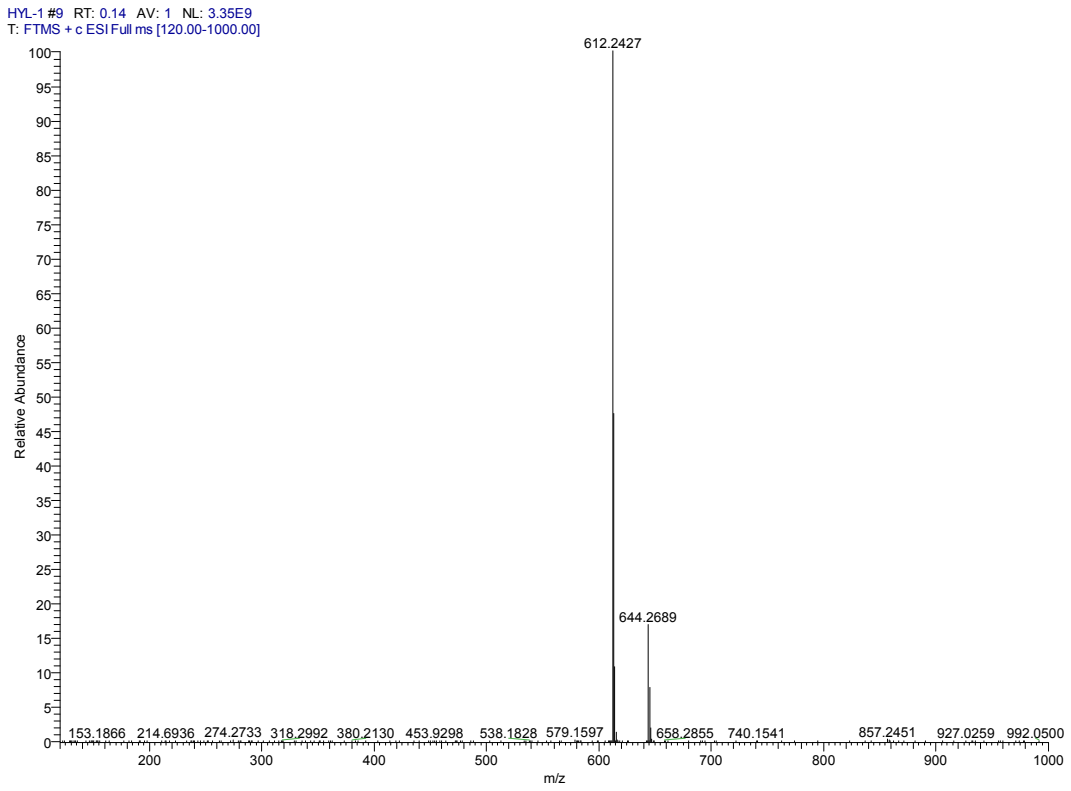

Fig. S32 ESI-MS mass original spectra of **Mito-SCHO**.

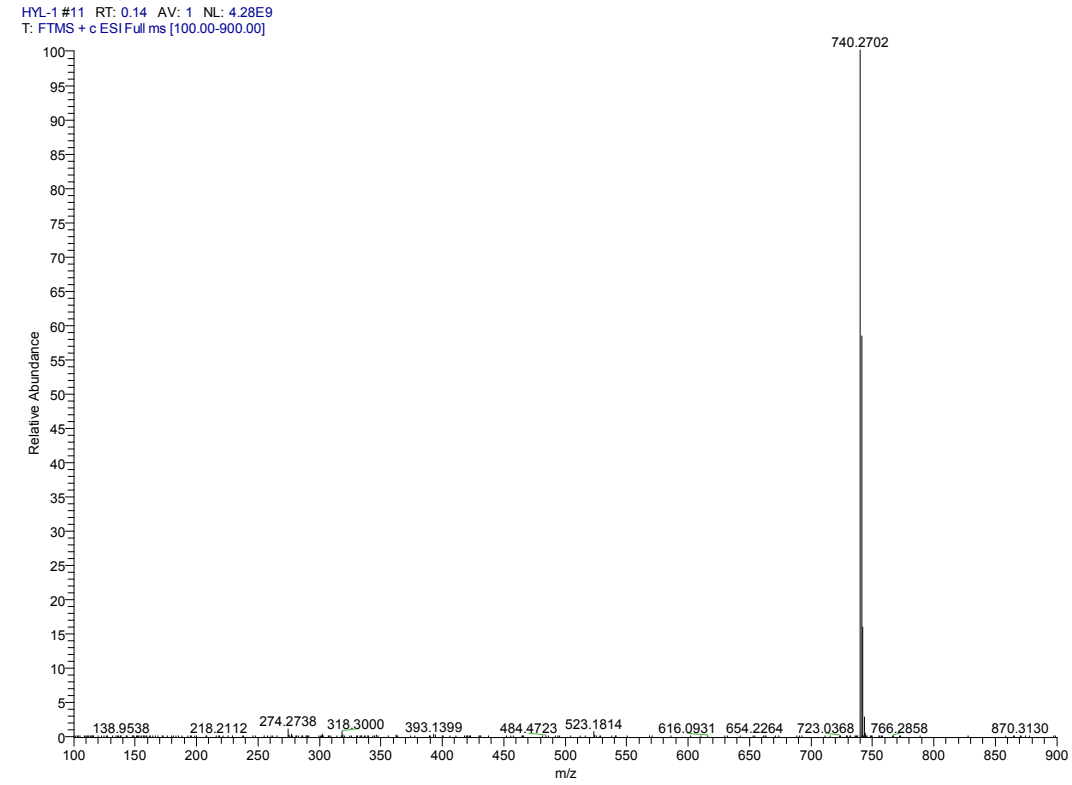

Fig. S33 ESI-MS mass original spectra of **Mito-DCHO**.

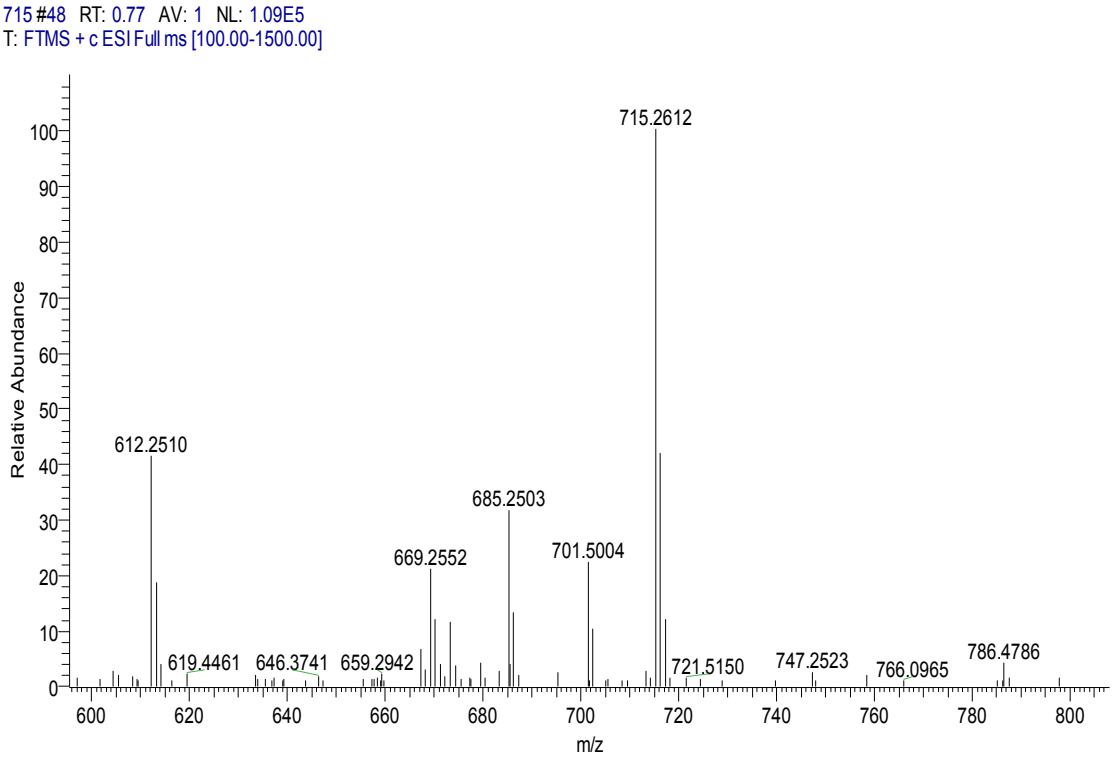

Fig. S34 ESI-MS mass original spectra of **Mito-SCHO-Cys**.

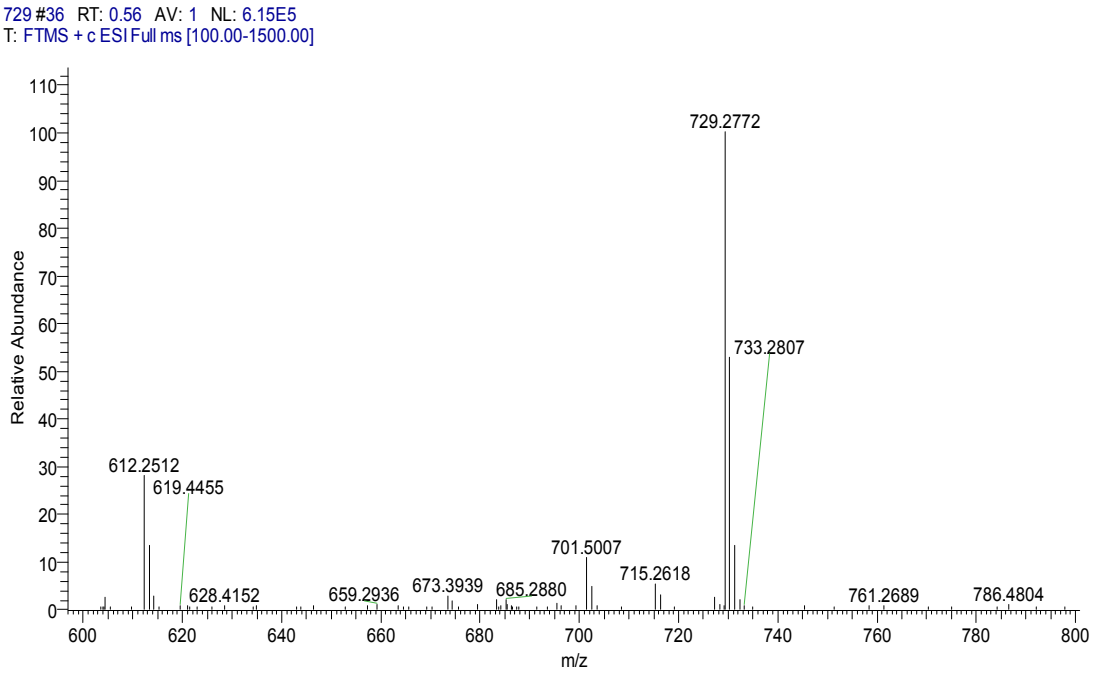

Fig. S35 ESI-MS mass original spectra of **Mito-SCHO-Hcy**.

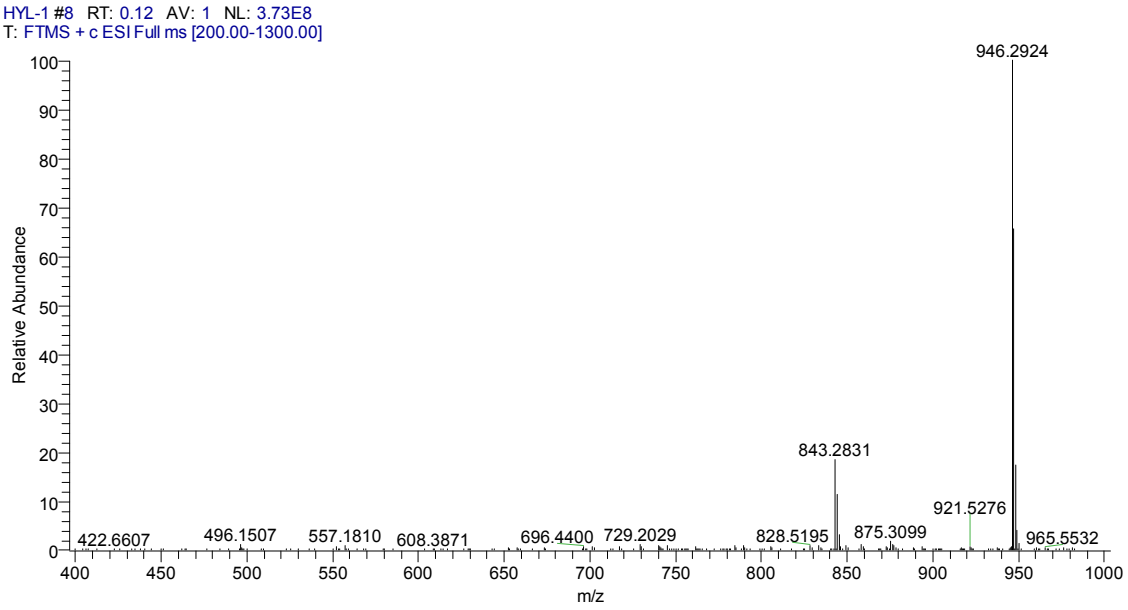

Fig. S36 ESI-MS mass original spectra of **Mito-DCHO-Cys**.